ChemComm

Luminescent MOFs (LMOFs): Recent Advancement Towards a Greener WLED Technology

Journal:	*ChemComm*
Manuscript ID	CC-FEA-06-2022-003330.R1
Article Type:	Feature Article

ARTICLE

Received 00th January 20xx,
Accepted 00th January 20xx

DOI: 10.1039/x0xx00000x

Luminescent MOFs (LMOFs): Recent Advancement Towards a Greener WLED Technology

Avishek Karmakar [a] and Jing Li [*a]

The replacement of the traditional incandescent, halogen and fluorescent lamps by white light emitting diodes (WLEDs) is expected to reduce the global electricity consumption by one-third by 2030, according to the US Department of Energy. The current WLED technology uses rare-earth element (REE) based phosphor materials, which, not only is cost-intensive but also constitutes an environmental concern. Hence, researchers are in quest for a new-generation of opto-electronic materials that can replace the conventional phosphors in WLEDs and thus aim towards a cleaner and more energy efficient lighting technology for the future. Luminescent metal-organic frameworks (LMOFs) have recently emerged as a new sub-class of MOFs which have demonstrated enormous potential for applications in sensing, imaging, optoelectronics and in solid-state lighting (SSL) technology. LMOFs could be game changers as lighting phosphors due to advantages such as high luminescence quantum yield, tunable excitation and emission which can be coaxed by rational design and optimization of metal centers, linkers, and the guest molecules, facile fabrication into devices, and structural robustness. These clear advantageous features of LMOFs make them score over the other contemporary materials, and render them futuristic phosphor materials for WLED technology. In this Feature article, we will provide an overview of the most recent developments of LMOF-based phosphor materials for SSL with a special focus on WLED technology. The emphasis will be centered around REE-free LMOFs, as the aim is to direct the attention of the readers towards a more viable and greener lighting technology.

1. Introduction

Carl Gustav Jung, a famous Swiss psychiatrist once said, “where there is light, there must be shadow, and where there is shadow there must be light”. Light has become indispensable part of human life since the first torch was lit 500,000 years ago. Artificial lights which emanate from electric lamps consume about 20% of world’s total electricity.[1, 2] This is perhaps the “shadow” that Jung referred to, which is a direct outcome of the rise in global usage of artificial “light” with rapid industrialization and urbanization. It is therefore essential to bring down the electricity/energy consumption by turning to cleaner and greener lighting technologies. The traditional incandescent, halogen, fluorescent, and high-intensity discharge (HID) lamps, which are used in general lighting and illumination applications have various limitations that have significant impact on both the energy and environment sectors.[3, 4] For example, the traditional incandescent lamps emit light by heating the metal filament thermally to ~3000 °C to reach the incandescent state.[5, 6] The high energy requirement and low energy-conversion efficiency make incandescent lamps incompetent for usage for a sustainable future. On the other hand, even though fluorescent lamps have higher energy output and longer lifetime compared to incandescent bulbs, they suffer some intrinsic disadvantages such as higher production costs, and health/environmental concerns due to chemical leakage and susceptibility to degradation.[7] Thus, low energy consumption/higher lumens per watt values and longer lifetime are needed for the development of a sustainable lighting technology that can make the light generation much more energy-efficient and consequently, a widespread global impact in the energy domain.

[a] *Department of Chemistry and Chemical Biology, Rutgers University, 123 Bevier Road, Piscataway, NJ 08854, USA*
* Corresponding Author.
Electronic Supplementary Information (ESI) available: [details of any supplementary information available should be included here]. See DOI: 10.1039/x0xx00000x

ARTICLE

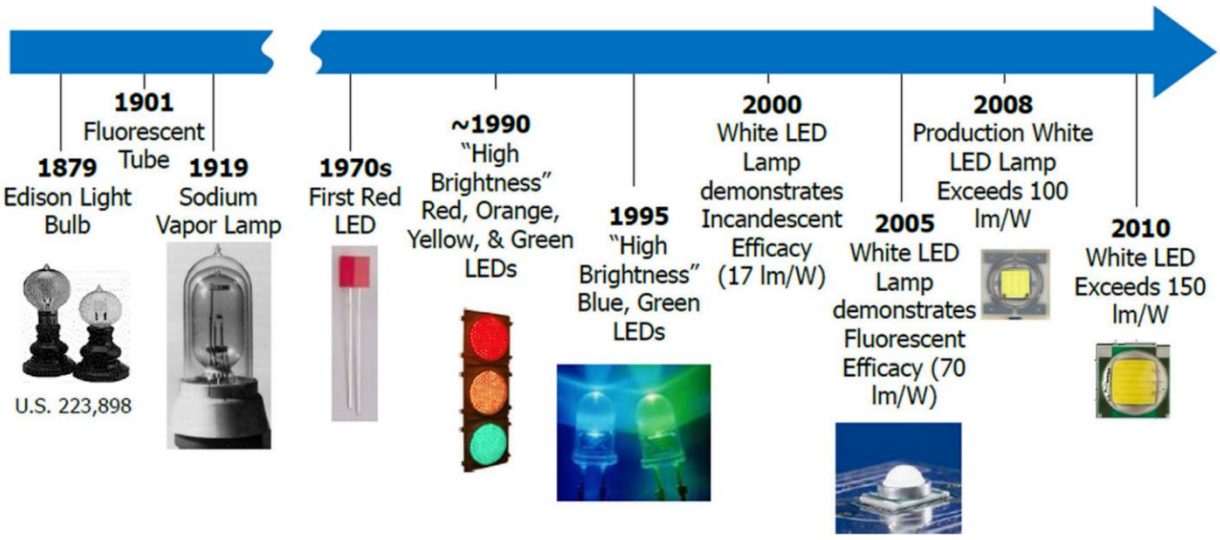

Figure 1: Timeline of development of various LED technologies and their luminous efficiency improvement over the period of time. WLEDs are the latest addition to this series. Reproduced from ref. 12 with permission from Elsevier, copyright 2014.

Solid-state lighting (SSL) is a relatively new lighting technology that is much more energy-efficient and longer-lasting compared to conventional light sources such as incandescent bulbs and fluorescent lamps. It serves as a viable solution to the future lighting needs.[8-12] According to the United States Department of Energy (DOE), States Department of Energy (DOE), adoption of advanced SSL technology could save 6.9 trillion kWh of energy equivalent to $710 billion and ~ 2 billion metric tons of CO_2 emissions by 2035.[13] As a most rapidly developing branch of SSL, LEDs have the potential to bring new functionalities to the modern lighting technology, thus, enhancing its applicability in a wide dimension of lighting systems which includes displays, signs, traffic lights, private households, industries etc.[14] In particular, significant progress has been made in the WLEDs in recent years due to their high efficiency, structural robustness, and longer lifetime (Figure 1). Since the discovery of WLED based on blue InGaN LED chip coated with YAG: Ce^{3+} phosphor,[15] strong research effort towards development of new phosphor materials has escalated.[16, 17] Typically, three main methods (Figure 2)[8] are used to generate white light in WLED technology: 1) three single LED chips (red, green and blue or RGB) are combined to generate white light, 2) an UV LED chip is used by exciting RGB phosphor materials to generate white light, and 3) in perhaps the most common method, a blue LED chip is used to excite a yellow phosphor material or multicomponent phosphor material(s) to produce white light.

Generally, phosphor converted WLEDs (PC-WLEDs) result in single, compact white light, but have some intrinsic disadvantages such as

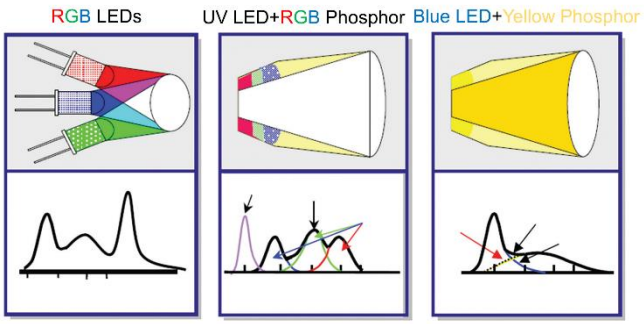

Figure 2: Conventional methods to produce white light. Blue LED+ yellow/multicomponent phosphor is the most common method used commercially. Reproduced from ref. 8 with permission from IEE, copyright 2002.

lower luminous efficiency and limited range of colour tunability owing to poor availability of phosphor materials.[18-20] The important metrics that determine the quality of light coming from a device include color temperature and chromaticity. Higher color temperature often signifies that an emissive material produces bluish white light whereas lower color temperature indicates that the emissive material produces warm yellowish white light.[21] The International Commission on Illumination (CIE) uses a chromaticity coordinate system to specify the color of light and has set the coordinates of equal-energy white as (x, y) = (0.33, 0.33).[22] For PC-WLEDs, rare earth element (REE) based inorganic materials such as

phosphates,[23, 24] silicates[25] and aluminates[26, 27] are used as phosphors. However, dependence on rare earth metals in such inorganic phosphors compromises on the sustainability of the technology because of the limited sources of such metals in the planet.[28] Also, the high temperature and high-cost synthesis that are usually required make their production less economic. Another very important issue that can't be ignored is the severe damages that their mining processes bring to the environment. Therefore, significant efforts are now devoted in minimising both energy and environmental footprints in WLED technology. Research in this domain has seen excellent progress towards the development of non-REE-containing phosphors for sustainable future. The past decade has witnessed an upsurge in the applications of some fascinating metal-organic frameworks (MOFs) in gas-storage/separation[29, 30], catalysis[31], drug-delivery[32] charge storage[33] and other key applications related to energy and environment. Luminescent MOFs (LMOFs) are a subclass of MOFs which have shown promising potential as fluorescent materials for chemical and biosensing[34, 35], light emitting diodes[36, 37], non-linear optics[38] and other optoelectronic applications. More recently, LMOFs have emerged as one of the yardstick materials for PC-WLED applications due to their excellent optical properties, tuneable architectures, and high physio-chemical stability.[39-41] The flexibility in design[42, 43] of these robust crystalline materials which includes availability of a wide plethora of metal ions/clusters and organic struts make them ideal candidates for future solid-state light emitting materials. Moreover, incorporation of emissive guest molecules such as dye, metal complexes, quantum/carbon dots etc. within the pores and/or post-synthetic modification in the organic backbone of the MOFs, render appropriate luminescence in LMOFs thus invoking desirable characteristics in terms of emission wavelength, frequencies, and quantum efficiencies.[44-46] Thus, LMOFs could be the potential gamechangers in the quest for finding REE-free phosphor materials for SSL and especially for WLED technology.

In this feature article, we aim to focus the attention of readers towards the progress of LMOFs as REE-free phosphor materials for WLED applications. The emphasis will be centered around REE-free LMOFs, as the goal is on the recent development towards a more viable and greener lighting technology. Progress of LMOFs for PC-WLEDs which have attracted increasing attention over the past several years will be highlighted. Ligand based emission strategies which can be achieved either by ligand charge transfer or by ligand rigidification, e.g., aggregation induced emission (AIE) will be discussed in detail. Charge transfer mechanisms involving ligand to metal charge transfer (LMCT) and metal to ligand charge transfer (MLCT) which are the key mechanisms influencing photoluminescence in LMOFs will be discussed with the focus on the aspects related to white light emission (WLE). Usage of single or multiple metal centered luminescence in solid-state lighting will also be discussed. Further usage of emissive guest molecules (e.g., dyes and metal complexes) which results in host-guest interaction within the MOFs and post-synthetic modification strategies (viz. ion exchange) will be covered. Lastly, the juxtaposition of important metrics with commercial viability (e.g., possibility of the fabrication of LMOFs into devices) will be reviewed.

2. Status of WLED technology

Recent years have proved to be a booming age for WLEDs due to their high efficiency, high CRI, low cost, and a universal technology. Organic/inorganic structures[47, 48], perovskites[49, 50], quantum dots (QDs)[51], MOFs[52] and other luminescent materials are being developed perpetually to the library of phosphors for this clean energy lighting technology. This field of research is growing and will continue to grow as researchers around the world are in quest for flexible, inexpensive, and energy/environmentally friendly and high efficiency phosphor materials which can substitute or replace the commercial REE-based phosphors. In the following subsections, we will briefly describe the typical methods of creating WLEDs/PC-WLEDs and summarize their advantages and disadvantages and the gap in the current research spectrum.

2.1. Blue-LED chip excitable phosphors

One of the simplest methods to produce dichromatic WLED is the use of a blue LED (e.g. InGaN) and a yellow phosphor (e.g. Ce^{3+} doped yttrium aluminum garnet, $Y_3Al_5O_{12}$). The emission spectrum is the combination of a narrow blue band originating from the blue LED with wavelength ranging between 450-470 nm and a broad yellow band originating from the phosphor material (YAG:Ce) (Figure 3a). The combination of blue and yellow light produces white light. By adjusting the ratio of the two emission bands, one can tune the correlated color temperature (CCT) of the white light generated. Figure 3b and 3c show two types of conversions in some phosphor-based WLEDs[53]. In a full conversion process, the phosphor is excited to higher energy levels upon excitation. During deexcitation, the phosphors emit red, green, and blue light which combine to generate white light.

Figure 3: a) Typical emission spectrum of YAG:Ce^{3+} phosphor based

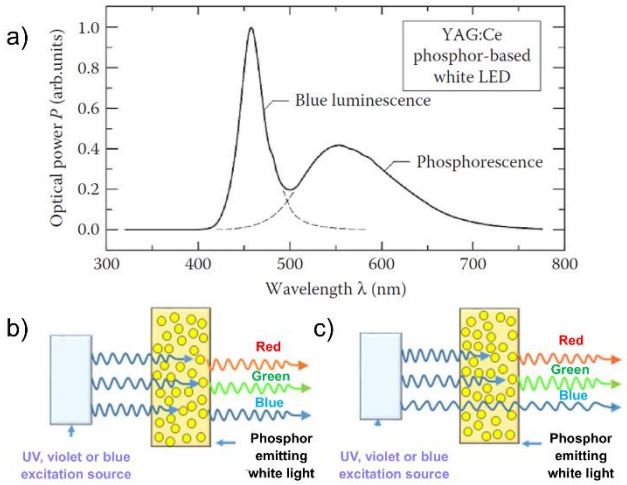

WLED produced by Nichia chemical industries corporation. Reproduced with permission from Schubert, E.F., Light-Emitting Diodes, Cambridge University Press, Cambridge, MA, 2003. b) Full conversion process, and c) partial conversion process in YAG:Ce^{3+} phosphor. Reproduced from ref. 53 with permission from IOP Science, copyright 2021.

In a partial conversion process, the phosphor material absorbs the blue light partially. The portion of blue light which is unabsorbed then combines with the red and green emitted light to yield white light. This technology first came to "light" in 1996 via a breakthrough discovery by Nichia and has changed the LED industry since then as it laid the foundation for development of cost effective, more efficient, high luminous efficiency and longer lifetime garnered LEDs. However, the relatively low CRI due to the absence of red spectral component and high CCT ≈ 7750 K have limited widespread acceptance of these systems as forerunners in current WLED industry.

2.2. UV-LED chip excitable phosphors

In this approach, a UV or near UV LED chip is used to excite red/green/blue phosphors to produce white light. Various commercial phosphors like $BaMgAl_{10}O_{17}:Eu^{2+}$ [54], $LiSrPO_4:Eu^{2+}$ [55] for blue emission, $SrAl_2O_4:Eu^{2+}$ [56], $(Ba, Sr)_2SiO_4: Eu^{2+}$ [57] for green and (Sr, Ca) $AlSiN_3: Eu^{2+}$ [58] for red and some other phosphate-based materials with general formula $ABPO_4$, (A = mono-valent cation and B = divalent cation) have been used extensively because of their hydrolytic and thermal stability. Although this method produces better CRI but suffers from disadvantages like lower energy efficiency due to loss during wavelength conversion. Moreover, from the economic standpoint, the cost associated with UV emitting cheap is much higher compared to blue excitable yellow phosphors.

2.3. Mixing RGB LEDs

LED chips of red/green/blue color when combined with an electronic circuit can, in principle, generate pure white light.[59] However, the high cost and complexity in changing the emission wavelength of individual chips (which would cause significant changes in the CCT) make this technology less viable for the future.

2.4. QD generated white light

More recently, white light produced by excitation of QDs has come to the limelight. QDs based on II–VI or III–V semiconductors and with a size range of 1-20 nm are marked by confinement effect of the electron-hole pairs in zero dimension.[60] The wide absorption range, sharp emission peaks and excellent quantum yields result in good color rendering of QDs. Also, by changing the elemental composition and the particle size, one can tune the emission characteristics of these QDs to generate suitable white-light properties. QDs can cover the entire visible range of spectrum and even the near IR or near UV range.

3. Luminescent MOFs (LMOFs) as "new-generation" smart phosphors

LMOFs have made a grand entry as phosphor materials for possible use in WLEDs due to their tunable architectures, changeable excitation and emission profiles through engineering appropriate metal ion/cluster, ligand, or functional guest molecule.[61-64] The long-range ordering and porous nature of LMOFs set them apart from the contemporary luminescent materials which are tested as phosphor materials. Moreover, the high chemical stability and structural rigidity of these framework materials allow longer lifetime, reusability and thus could be potential game-changers in the WLEDs. The origin of luminescence in LMOFs is briefly describe below.

In general, photoluminescence in LMOFs is caused by the emission of the photon from the excited state to ground state after the receptor has been excited by absorption of light.[35, 65] There are two ways by which the photo-induced excited state reverts to ground state: 1) Fluorescence - in which the electron is excited to a singlet excited state (S_n) upon shining light and then relaxes to lowest excited singlet state (S_1). The emission occurs when the electron transfers from S_1 to the ground state (S_0) via a spin allowed transition. This process is usually fast and is in the order of nanoseconds to microseconds. 2) Phosphorescence - in which upon excitation, the electron jumps from ground state to S_n. However, during relaxation process, the electron makes a transition from the lowest excited state (S_1) to a triplet excited state (T_1) via an intersystem crossing. The electron then proceeds to a transition from T_1 to the ground state (S_0) via a spin forbidden state. Phosphorescence is usually a slower process as compared to fluorescence due to the spin forbidden emissive transition and can be in the order of milliseconds to seconds (Scheme 1).

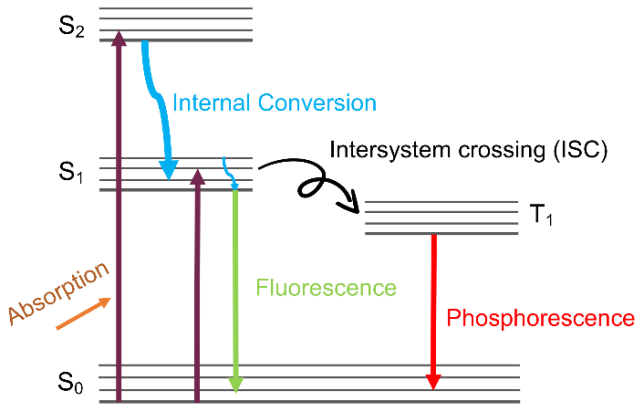

Scheme 1: Scheme showing various photophysical processes in a phosphor system after absorption of light.

The color of the light emitted from the material depends on the bandgap. Quantum yield governs the efficiency of the photoluminescence process. The internal quantum yield (IQY) is the ratio of emitted photons to absorbed photons, whereas the external quantum yield (EQY) is the ratio of emitted photons to incident photons.[66]

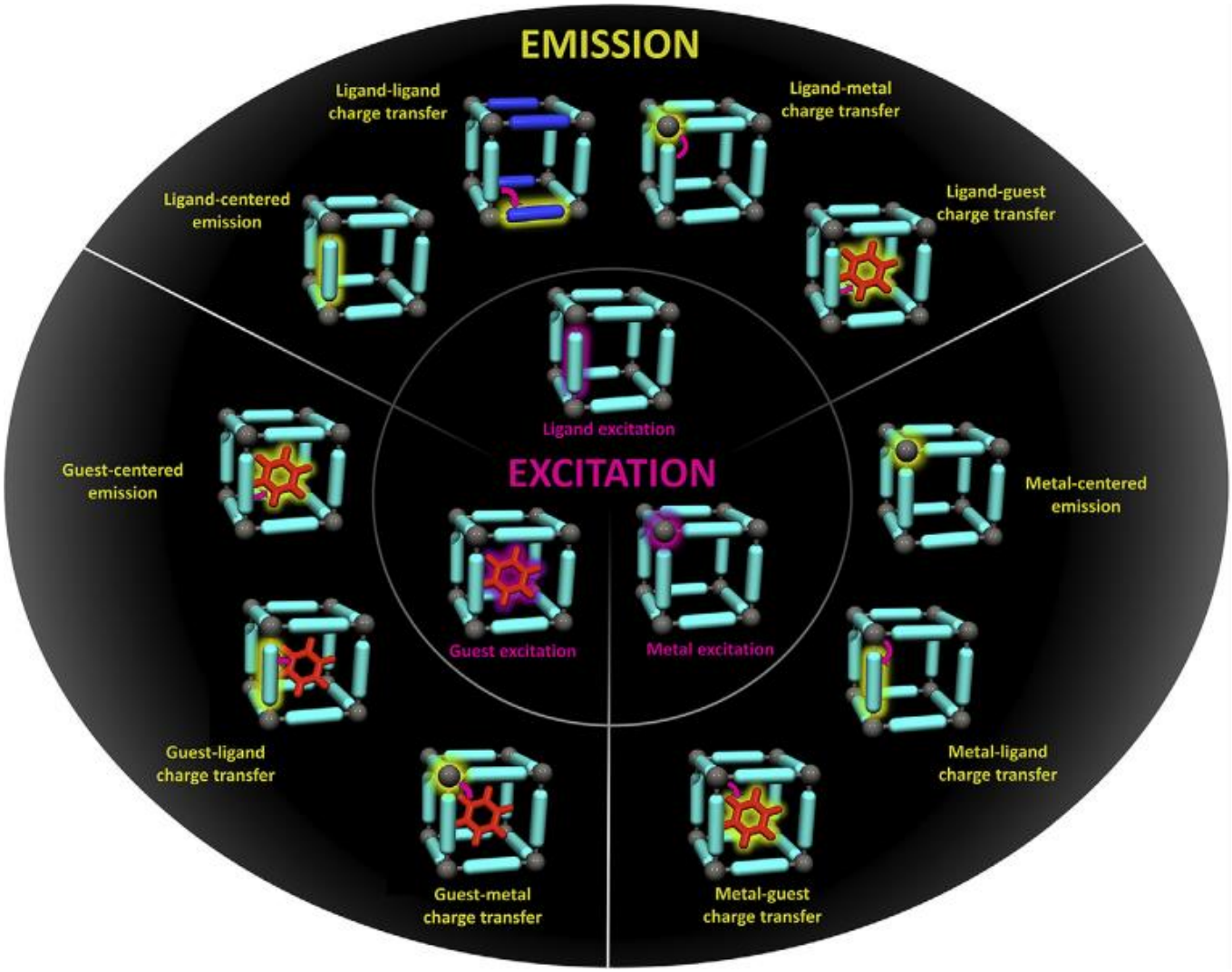

Figure 4: Illustration showing the details of various processes occurring in LMOFs with the ligand, metal and guest species all contributing towards luminescence. Reproduced from ref. 67 with permission from Elsevier, copyright 2018.

The three main responsible units for the luminescence in MOFs are the organic ligands, metal ions and guest molecules within the pores of MOFs (Figure 4). They result in various processes including a) ligand-based emission, b) ligand to ligand charge transfer (LLCT), c) ligand to metal charge transfer (LMCT), d) metal-based emission, e) metal to ligand charge transfer (MLCT) and finally, f) guest induced luminescence.[67] π-electron conjugated organic ligands often contribute to the emission of LMOFs.[68] The ordered immobilized arrangement of these electron rich ligands within the backbone of the MOFs results in reduced non-radiative decay and hence higher quantum yield in LMOFs. LLCT occurs because of compact spatial distribution of the organic ligands in the MOF framework which facilitates the charge transfer between the ligands.[69] In case of LMCT, the lone pair(s) of the ligand which are at higher energy donates electrons to low lying vacant orbitals of the metal ion. Conversely, in MLCT the electron density flows from the fully filled metal bonding orbitals to the vacant π* orbitals of the ligand (typically aromatic ligands).[70]

Generally speaking, the mechanisms that govern such electron/charge transfers in LMOFs depend on the electronic structure of the metal ions and ligand which determines the energy difference between the highest occupied molecular orbital (HOMO) and lowest unoccupied molecular orbital (LUMO) of the MOF. For example, to achieve a high-efficiency ligand-based LMOF phosphor, judicious design of ligand is of paramount importance. Organic ligands based on AIE[71] are specifically one of the main proponents for inducing tunable and high luminescence in MOFs. Rigid ligands with considerable π electron density have limited molecular rotations and exhibit unique fluorescence properties due to distinct energy conformations in porous space. As a result, in ligand-centered

ARTICLE

luminescence, increased quantum yield and tunable color emission are generally obtained.

In metal-centered luminescence, lanthanide ions which have sharp f-f transitions, have characteristic color associated which such electronic transitions.[72, 73] For example, Tm(III), Er(III), Ho(III), Sm(III), and Pr(III) based MOFs emit light at various frequencies in the visible light spectrum. Specifically, Eu(III) shows emissions in the orange-red region, Tb(III) in the yellowish green region, and Dy (III) in the bluish-green region. Since f-f transitions are Laporte forbidden, the absorption of the lanthanide ions is generally poor as observed from their weak luminescence under direct excitation. The presence of strongly absorbing organic ligands in MOFs act as sensitizers for the lanthanide atoms via "antenna effect" thus boosting the luminescence efficiency. [74]

In guest-induced luminescence, fluorescent dye molecules, metal complexes, QDs, etc. are generally incorporated inside the pores of the framework either in-situ or via post-synthetic modification procedures to generate white light.[75] These guest molecules can either dominate the overall emission characteristics of LMOFs or compliment the emission coming from the framework.

In the subsequent sections, we will discuss in more details about the specific examples of LMOFs and their WLED based applications. We will purposefully limit our discussion to REE-free LMOF phosphors as the development of such materials is of vital importance towards greener WLED technology.

3.1. Photoluminescent MOFs (PL-MOFs) as REE-free phosphors

Most of the early literature is dominated by REE-based LMOFs for white light generation.[76] However, as mentioned previously, due the limited resources, economics associated with them and the adverse environmental effects of REEs, such WLED technology may not be suitable for a sustainable future. MOF researchers have targeted this problem and have come up with novel strategies to design REE-free phosphor materials for WLEDs. These include designing PL-MOFs based on novel chromophore-based ligands, or by various charge-transfer, or by incorporation of multiple emission centers within the framework. These methods have been useful in efficient white light generation which satisfy the metrics such as CRI, CCT, IQY, EQY, CIE coordinates etc.

3.1.1. AIE based PL-MOFs for white light emission

Installation and immobilization of chromophore ligands in MOFs has turned out to be a very effective way for generating white light.[77, 78] By using conjugated chromophoric ligands along with metal centers that contribute solely as nodes during MOF synthesis, highly emissive LMOFs can be constructed which not only have ligand-based emission but also exhibit enhanced luminescence due to rigidification of the ligand (reduced molecular motions such as vibrations and rotations). In this regard, MOFs with aggregation induced emission (AIE) properties have emerged as a distinguishable platform for studying intra- and intermolecular interactions in chromo-luminescence. AIE-MOFs[79, 80] show programmable output signals as a function of both ligand structure and interaction and have switchable photophysical properties. It has been shown that an otherwise non-emissive ligand can lighten up after coordinating with the metal ions via matrix coordination-induced emission effect (MCIE)[81] . Thus, by donor-acceptor based strategy in chromophoric linker and metal nodes with non-linear optics such as lanthanides or REEs, the resulting MOF could show desirable emission. Tetraphenyl ethylene (TPE) core is well known in literature for AIE based fluorescent properties.[82] By increasing the arm length of the TPE core, the bandgap and emission color of the ligand and resulting MOFs can be tuned.[83] However, one limitation of single chromophore-based LMOF is the lack of emission energy tunability, as the emission energy of such structures is fixed with a given ligand. To lift such a limitation, Li and co-workers developed a strategy by introducing second ligand, so called bandgap modulator, to tune the emission color.[84] $[Zn_6(btc)_4(tppe)_2(DMA)_2]\cdot 9DMA\cdot 12H_2O$ was designed in such a way by incorporating 1,1,2,2-tetrakis(4-(pyridin-4-yl)phenyl)ethene (tppe, as chromophore ligand) and 1,3,5-benzentricarboxylate (btc, as modulating ligand)[84] (Figure 5a). While tppe itself emits green light, the emission of this MOF is red-shifted to give yellow color (Figure 5b) with an IQY of 90.7% which was among the highest reported values of all REE-free yellow phosphors. In later studies by the same group[85-88] the authors demonstrated their linker engineering approach by several other examples. 1,2,2-tetrakis (4-(4-carboxy-phenyl) phenyl) ethene (H_4tcbpe), 1,1,2,2-tetrakis(4-(4-carboxy-3-fluoro-phenyl)phenyl)ethene] (H_4tcbpe-F) and 1,1,2,2-tetrakis [4-(pyridin-4-yl) phenyl] ethene (tppe) were used as chromophore ligands in combination of various modulating ligands to achieve different emission colors. Figure 6 shows two LMOFs, LMOF-231 (single chromophore ligand) and LMOF-241 (chromophore and modulating ligand), both are based on Zn^{2+} metal cation.[85] Both MOFs exhibit high IQY and excellent thermal stability as a result of the rigid backbone present in the frameworks. A luminous efficacy of 58.9 ± 1.5 lm W^{-1} was

achieved for a prototype PC-WLED based on guest-free LMOF-231 as phosphor, which is above the standard set by US EPA's ENERGY STAR program for omnidirectional lamps.[87] In addition, the authors have also shown that by substituting pristine ligand H_4tcbpe with fluorine functionalized H_4tcbpe-F to produce a semi-fluorinated analogue of LMOF-231, LMOF-305, an IQY of 88% (λ_{em} = 550 nm at 455 nm excitation) was achieved, setting a record for luminescent efficiency in yellow-emitting, blue-excitable, REE-free LMOF phosphors.[89] Very recently, Huang, Li and co-workers constructed a LMOF from Ca^{2+} and tcbpe-F ligand which emits yellow light with a quantum yield of 68%.[90] The authors demonstrated guest induced structural transformation via water incorporation due to high hydration energy of the MOF. The phase-changed MOF thereafter showed red shift in the

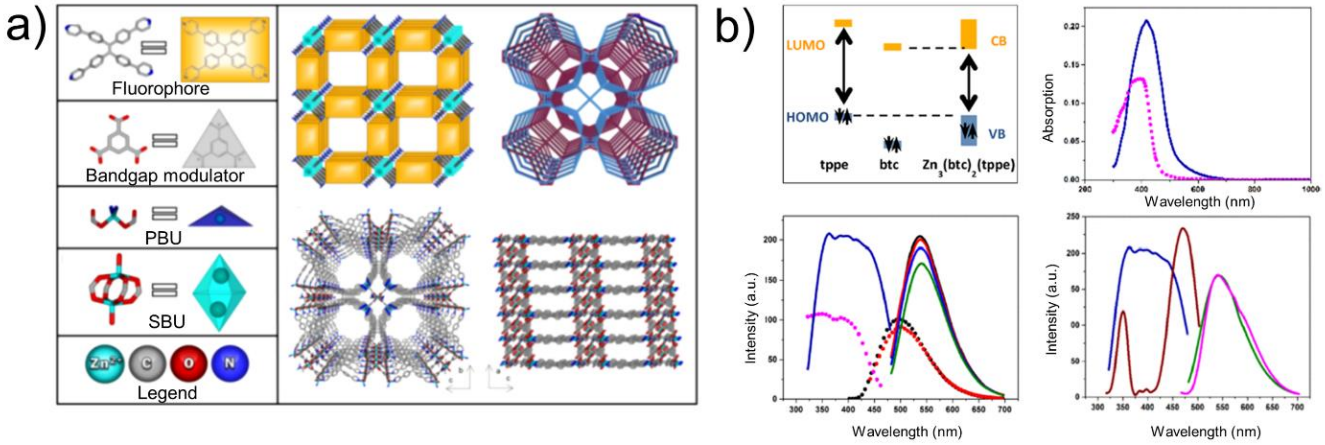

Figure 5: a) Building units of MOF showing the structure of tppe ligand, btc (red shift modulator), primary building unit (PBU) and the secondary building unit (SBU) resulting in the formation of 3D porous of $[Zn_6(btc)_4(tppe)_2(DMA)_2]$ which are porous from a and b axis. b) Optical properties of the ligands and the MOF showing bandgap, absorption profile (pink dotted line for tppe and blue for MOF) and photoluminescence profile (down left) showing dotted lines for tppe and solid lines for MOF at different excitation wavelengths. The photoluminescence profile of the MOF was also compared to that of YAG:Ce^{3+} phosphor at different excitation wavelengths (down right). Reproduced from ref. 84 with permission from American Chemical Society, copyright 2014.

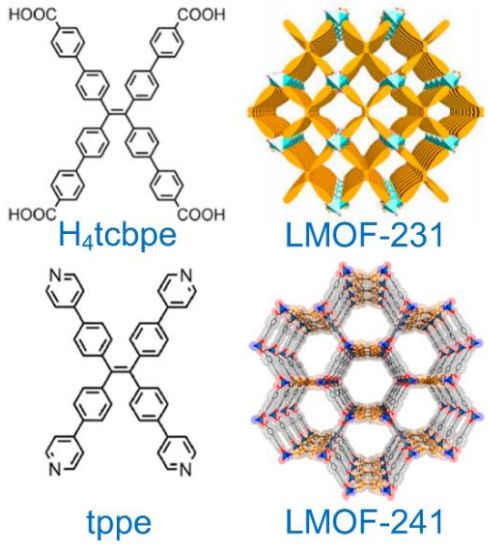

Figure 6: AIE based ligands, H_4tcbpe and tppe result in the formation of LMOF-231 and LMOF-241. Reproduced from ref. 85 and ref. 86 with permission from American Chemical Society, copyright 2016 and from American Chemical Society, copyright 2015.

emission profile as compared to the parent MOF. This is the first calcium-based MOF that emits yellow light at 550 nm under blue light excitation. Wang et al.[91] constructed two Zn based LMOFs based on a chromophore, [tri(4-pyridylphenyl) amine] (tppa) and two co-ligands, viz. 2,6-naphthalenedicarboxylic acid (ndc) and (E)-4,4'-(ethene-1,2-diyl) dibenzoic acid (sdc). Both MOFs showed strong yellow emission under blue excitation and the CIE coordinates were close to the of YAG: Ce^{3+} phosphor. The MOFs when dispersed in ethyl acetate and coated on a blue LED chip produced white light. 1,2-bis(4-(4-carboxyphenyl))-1,2-diphenylethene (H_2BCPPE) which is a strong chromophoric ligand was exchanged into bio-MOF-101 via solvent assisted ligand exchange (SALE) strategy. The resulting MOF, bio-MOF-101-BCPPE showed a greenish blue emission at 491 nm when excited by blue light (375 nm). The quantum yield for this LMOF was estimated to be 42% with CIE coordinates of (0.35,0.36).[92] A metal–organic layer (MOL) which is derived from a MOF by reducing one dimension into single/few layers are important candidates in designing 2D luminescent materials for WLEDs. Hu et al.[93] reported a 2D MOL (Zr-TCBPE-MOL) with a secondary building unit of $[Zr_6O_4(OH)_6(H_2O)_2(HCO_2)_6]^{4+}$ and H_4tcbpe linker (Figure 7a, b). The ultrathin nanosheets (Figure 7c) can immobilize fluorescent struts which prevents self-aggregation and

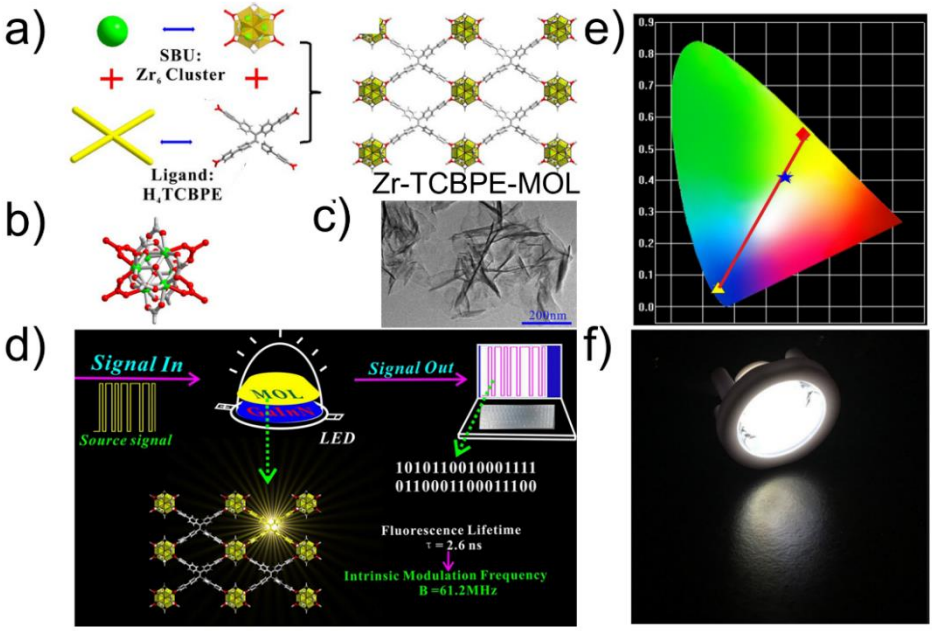

Figure 7: a) Building units of the Z-TCBPE-MOL MOF showing the structure of H4tcbpe and Zr6 cluster based SBU forming the resulting MOF. b) Ball and stick model of the rigid SBU. c) HR-TEM image of the Z-TCBPE-MOL. d) Schematic representation of the VLC performance by the MOF. e) CIE coordinates of the MO based WLED (red square shows Zr-TCBPE-MOL, yellow triangle shows a 450 nm LED and blue star shows MOL-WLED). f) Image showing MOL-LED. Reproduced from ref. 93 with permission from John Wiley & Sons, copyright 2017.

molecular motions resulting in manifold increase in the fluorescent properties. The MOL emits yellow light with a wavelength of 560 nm when excited with a light of wavelength 450 nm with a CIE coordinate of (0.42, 0.54) (Figure 7e). The fluorescence lifetime for this material was about 2.6 ns which indicates that WLED fabricated from this material can be turned on/off faster than commercial ones. The quantum yield for this material was reported to be 50% which is suitable for device development (Figure 7f). The MOL material was further tested for visible light communication (VLC) (Figure 7d) which afforded a physical switching speed (PSS) three times that of commercial WLEDs. Thus, overall, this material had the potential to replace the commercial YAG: Ce^{3+}in commercial lighting.

3.1.2. White-emitting PL-MOFs based on charge-transfer

Charge transfer processes such as LLCT, MLCT, LMCT are responsible for significant luminescent characteristics in LMOFs.[94-96] As the HOMO-LUMO energy gaps of the LMOFs are greatly affected by the nature of the metal ion, ligand, coordination geometry, local environment around the SBU etc., one can change or play around with multiple controlling factors to tune the emissive properties of such LMOFs. Atomic level engineering in LMOFs is one of the reasons for the tremendous potential of these materials in various opto-electronic applications, as, often, intricate level system designing is necessary to extract highest performance in terms of emission wavelengths, quantum efficiency, lifetime etc. Thus, suitable phosphor materials can be designed based on the judicious choice of metals and ligands, ration synthesis protocols, and based on structure-property correlations. In of the earlier reports, Guo and his group members[97] reported a silver metal ion based LMOF, $[AgL]_n \cdot nH_2O$, where L = 4-cyanobenzoate. The compound shows tunable yellow to white emission. Each Ag atom is coordinated by two O atoms from the carboxylate groups and one N atom from the cyano group resulting in a near T shaped configuration. The wavy 2D nature of the structure is highlighted by the Ag-Ag distance of 2.8303 Å in the $[Ag_2(O_2C)_2]$ cluster, strong π-π interaction between the layers and weaker Ag...Ag interaction. The compound shows emission at ~427 nm and ~566 nm under 355 nm excitation. The authors found that

with the decrease of the excitation wavelength, the intensity of the 427 nm peak also decreases but enhances emission at 513 nm, 566 nm and 617 nm which generates yellow light. When the excitation energy was adjusted to ~350 nm, the emissions at 427 nm and 566 nm become comparable in intensity, resulting in white light (Figure 8).

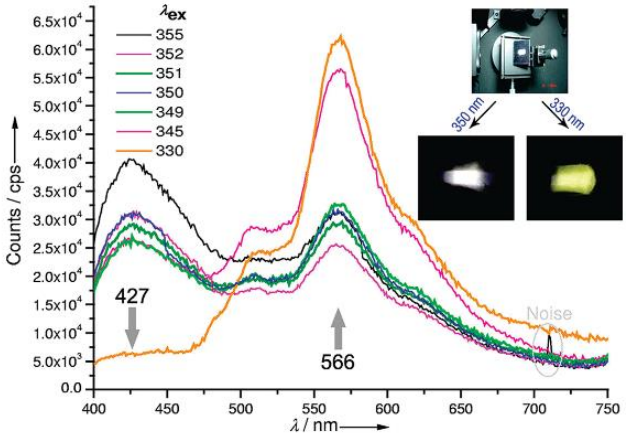

Figure 8: Emission spectra of $[AgL]_n \cdot nH_2O$. Tuneable yellow to white emission in WLED device. Reproduced from ref. 97 with permission from American Chemical Society, copyright 2009.

Thus, tunable yellow to white light generation was possible in this case. The CIE coordinates are (0.31, 0.33) with a quantum efficiency of ~10%. The authors predicted that both ligand-centered emission and MLCT are responsible for this MOF. Xu et al.[98] reported coordination polymers based on Ir(III) polypyridine complexes and alkaline-earth metal (Mg). The distinctive emission peaks are a result of Ir(III) unit which leads to MLCT and LLCT that occur in such coordination polymers. The authors also concluded that different solvent molecules in such complexes also play important role in the emission properties. More recently, Pb^{2+} based MOFs have been explored for white light generation based on (1) Pb^{2+} -based s→p transition, (2) LMCT, (3) MLCT and (4) Pb^{2+} influenced π→π* transition. Pb^{2+} based MOF have been used as single phase WLE materials and have shown to produce white light with high CRI and quantum yield. Such MOFs could potentially exceed the Pb-based perovskite materials for WLE because of higher physio-chemical stability, higher IQY/EQY and better scaling up synthesis procedures for implementation in devices. For example, Chengdong et al.[99] designed two 3D lead bromide frameworks (TJU-6 and TJU-7) that produced broadband white light of ECQ up to 5.6% and CCT of 5727 K. The overall charge in these frameworks is positive which induces high distortion of the Pb^{2+} centers, thus generating self-trapped states. Under illumination at 365 nm, these frameworks showed broadband luminescence which spans between 400-700 nm (Figure 9).

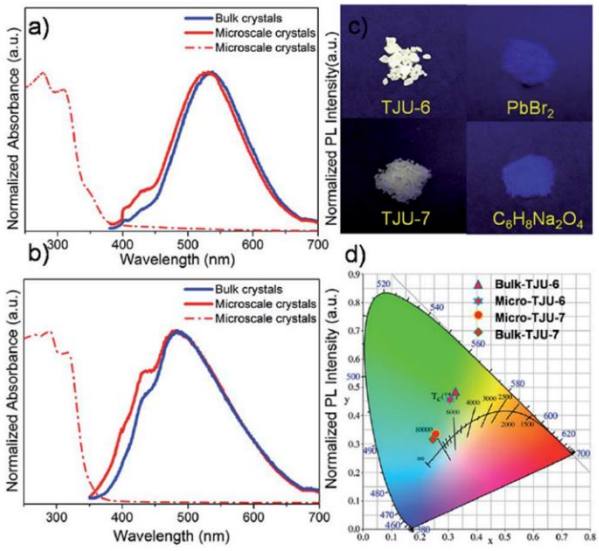

Figure 9: a) Emission spectra of TJU-6 and b) Emission spectra of TJU-7. c) White light emission under UV light properties of TJU compounds and comparison with precursors. d) CIE coordinates mapping of TJU-6 and TJU-7. Reproduced from ref. 99 with permission from The Royal Society of Chemistry, copyright 2018.

The stable nature of these compounds and higher quantum yields as compared to Pb perovskite-based materials for WL generation opened avenues to fabricate new phosphor materials for single phase WLE. Al-Nubi et al.[101] synthesized new Pb-based MOFs with formula $Pb(HL_3)(1,4\text{-dioxane})_{0.5}$ and $Pb_2(HL_3)_2(H_2O)_5$ (H_3L_3 = benzene-1,3,5-tricarboxylic acid, btc) which showed distinct difference in the luminescence spectra as compared to the btc ligands possibly due to the combination of LLCT, MLCT and LMCT occurring in these ordered structures. When excited at 350 nm, $Pb(HL_3)(1,4\text{-dioxane})_{0.5}$ showed a greenish yellow emission, whereas, $Pb_2(HL_3)_2(H_2O)_5$ showed near white light emission. The CIE coordinates of (0.33, 0.36) was close to the ideal CIE coordinates (0.33, 0.33) for white light emission. Although the origin of the luminescence in these Pb-based frameworks are mostly ascribed to $[Pb_2X^{3+}]$ units, the rigid dicarboxylate linker also contributes to the ligand-centered emission which further enhances the luminescent properties of these charged frameworks. Lin et al.[100] demonstrated cationic $(Pb_4X_2)^{6+}$ based 1D chains and rigid 2,6-naphthalene dicarboxylic acid (ndc) ligands for the construction of 3D cationic frameworks viz. $[(Pb_4X_2)\ (ndc)_4 \cdot A_2]_n$ where X is Cl, Br, and I, A is $(CH_3)_3NH^+$ and $(CH_3)_2NH_2^+$). The bromo- and iodo-derivatives showed WLE which was a result of the ligand centered blue emission and the red emission from the haloplumbate centers. Three stable WLE MOFs with general formula: $[Pb_2X_3^+]\ [L_7]_2\ [(CH_3)_2NH_2^+]_3$ where X = Cl/Br/I) and L = 1,4-benzenedicarboxylate upon near UV excitation, exhibited

broadband emission with CRI ~ 89.[102] Secondary group participation (SGP) of $CH_3SCH_2CH_2S^-$ and (S)-$CH_3(OH)CHCH_2S^-$ (2-hydroxylpropyl) modified bdc linkers at the 2 and 5 positions yielded two emissive Pb-based frameworks with yellowish green and bright white light respectively.[103] The reasons were attributed to LMCT in the case of $CH_3SCH_2CH_2S^-$ decorated framework, while in the 2-hydroxylpropyl modified framework LMCT and s→p transitions contribute to the white light generation. Usman et al.[104] reported a three-dimensional (3D) Sr-based LMOF, $[Sr(Hbtc)(H_2O)]_n$, which showed typical semiconductor behavior with a bandgap of 2.3 eV which was comparable to commonly known semiconductor materials like CdSe, CdTe, ZnTe, GaP. When this MOF was illuminated by a 266 nm pulsed laser, it showed two distinct photoluminescent emissions at ~330 and 640 nm. The peak at 330 nm was attributed to the ligand centered emission, whereas the one at 640 nm was due to LMCT process occurring in the MOF. A luminescent coordination polymer (LCP) based on $BiBr_4$ and a neutral zwitterionic ligand (N-oxide-4,4'-bipyridine) formed a linear 1D chain and the resulting negative charge was balanced by the tetrabutyl ammonium (TBA) cation.[105] Under UV excitation, the LCP exhibited yellow emission (540 nm) with a lifetime of 18µs. The longer lifetime was possibly due to the phosphorescence process occurring due to the heavier Bi atom. DFT calculations predicted the lowest energy excitation process to be due to the charge transfer process from the $BiBr_4$ cluster to the ligand. Li et al.[106] reported a π-electron rich ligand 4-(tetrazol-5-yl) phenyl-2,2':6',2''-terpyridine (Htzphtpy), which in combination with Cd^{2+} yielded 1D chains of $[Cd(tzphtpy)_2] \cdot 6.5H_2O$. Strong π- π interactions between the ligand of a single chain and LLCT between multiple chains resulted in emissions at 454 nm and 554 nm respectively. Under UV excitation at 326 nm the generated white light with CIE coordinates of (0.33, 0.36). The authors observed that as the excitation wavelength increases, the ligand cantered emission decreases and the LLCT increases.

3.1.3. PL-MOFs with multiple emission centers

In this section, we will give a brief summary of the multiple emission center based LMOFs for rendering white light. The chemistry of LMOFs and is complex yet fascinating. As mentioned earlier, the origin of photoluminescence in LMOFs can be localized on one of the components (metal ions/ organic ligands/guest molecules). More recently, systematic tuning of multi-component luminescence has attracted the attention of researchers to regulate the emission characteristics of LMOFs.[107-109] In multiple emission process, simultaneous participation of functional emissive/non-emissive groups[110] (Figure 10) offers a platform for a wide variety of applications including fluorescence sensing, ratiometric titration, anti-counterfeiting, WLEDs, bio-imaging etc.

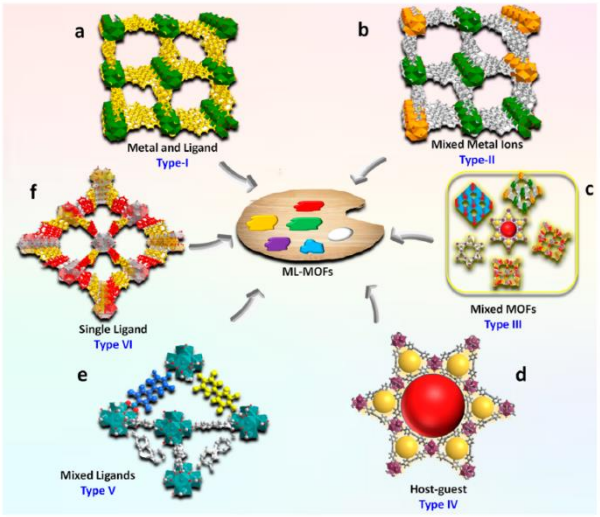

Figure 10: Illustration showing various contributing factors towards multi-emission process in MOFs. In all the process the metal ion/ligand /guest species play a central role. Reproduced from ref. 110 with permission from American Chemical Society, copyright 2020.

One focused area of this research is around usage of green emitting Tb (III) and red emitting Eu (III) which combine with the blue emitting MOF framework to produce white light. The balancing stoichiometric ratios of the lanthanide ions in the composite material is crucial in this aspect to blend the emissions from the individual components for white light. LMOFs with blue emission originating from the ligand has been coupled with La (III) or Gd (III) to secure the ligand-centered emission. Such MOFs are then doped with Tb (III) and Eu (III) to obtain suitable color mixing for white light emission.[111, 112] However, one of the drawbacks for such methodology is that they have low CRI due to the sharp emission originating from the lanthanide ions. Moreover, from the environment and energy perspectives, this method has some drawbacks and is not a solution for sustainable future.

In developing REE-free phosphors, there are a number of ways to introduce multiple emission centers of a LMOF to generate white light. These include: i) dye molecule incorporation, ii) emissive inorganic complex/QDs incorporation and, iii) linker functionalization with variable color profiles. Since majority, if not all, such processes include host-guest interactions, choosing suitable MOFs with guest interacting sites and guest molecules with appropriate electronic properties are essential for achieving the maximum output signals. Also, the porosity of MOFs must be taken into consideration as the framework structure should be sufficiently porous to allow facile diffusion of foreign species into the cavities of MOFs to allow host-guest interaction. Since MOFs have a high degree of structural flexibility and chemical tunability, these approaches are often useful to generate white light emission in a much more effective and compact manner. In the following discussion, we will discuss each method more closely to give the readers a fair

knowledge about the design strategies and applications of such LMOFs with multiple emission centers.

Dye incorporation in LMOFs: Organic dye molecules with planar electronic structure have known to emit in dilute solutions rather than in solid state because of intermolecular quenching interactions in solid state like π- π stacking.[113-115] Dye encapsulated in MOFs is an efficient method to restore the emission properties of dyes in solid-state because of restricted aggregation caused quenching (ACQ) of the dyes by confinement effect inside the pores of the MOFs.[116] Such dye@MOF composites thus have been used efficiently for generation of pure white light with high quantum efficiency and CRI. A list of some common dyes which have been encapsulated in MOF structures for various opto-electronic applications including WLE is given in Figure 11.

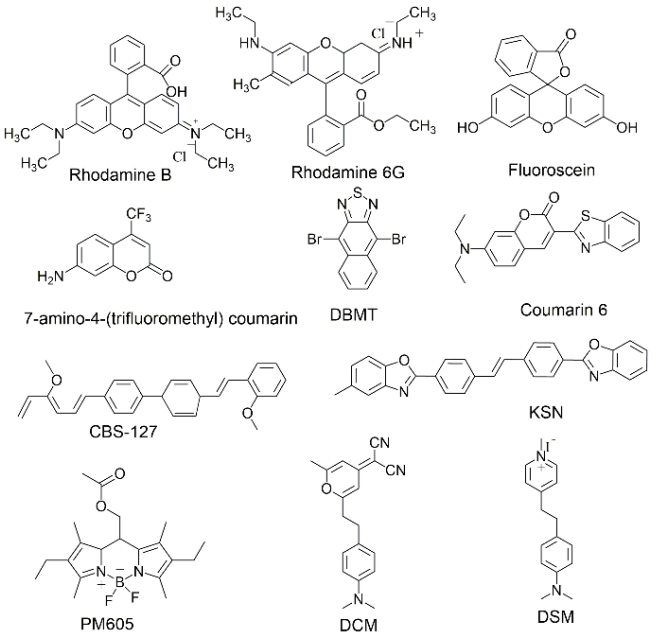

Figure 11: List of common dye molecules which have been incorporated in the MOF structures for various opto-electronic applications.

In perhaps the first report of this strategy in 2015, Cui et al.[117] reported that both the red and green emitting dyes, viz., 4-(p -dimethylaminostyryl)-1-methylpyridinium (DSM) acriflavine (AF) could be inserted in a blue emitting anionic LMOF i.e., ZJU-28 by cation exchange process. The DMA cations were readily exchanged by these cationic dyes in solution to yield ZJU-28⊃DSM, ZJU-28⊃AF and ZJU-28⊃DSM/AF, depending on the nature of the dye encapsulated in the pore-structure. The ZJU-28 emission which showed blue emission at 415 nm gradually changed to red and green emission as the loading of the DSM and AF increases in the ZJU-28⊃dye composites. Thus, the color of the MOF⊃dye composites could be tuned depending on the nature of the dye chosen for exchange. To fabricate a WLED device, the authors synthesized ZJU-28⊃DSM/AF, in which both DSM and AF were incorporated inside the MOF with varying soaking time and dye concentration. The optimal dye loading of 0.02 wt% and 0.06 wt% of DSM and AF were found to be suitable for white light emission. The quantum yield of this composite was found to be 17.4% with CCT and CRI values as determined were 5327K and 91 respectively. The CIE coordinates were estimated to be (0.34, 0.32) respectively. In order to check the working performance, the authors coated the solution processed MOF⊃dye on 365 nm ultraviolet LED chip and generated bright white light. Wang et al.[118] demonstrated that warm white light could be generated in rhodamine B dyes encapsulated in an Al-DBA MOF (DBA = 9,10-dibenzoate anthracene). The resulting composite material i.e., RhB@Al-DBA produced white light by combining the blue emission of DBA and the yellow emission of rhodamine B dyes. The significant energy transfer from the MOF to the dye molecules caused dual emission in the composite structure. The lifetime for the blue and yellow components in the MOF⊃dye composites are 1.8 and 5.3 ns respectively, which are significantly shorter than the commercial $Y_3Al_5O_{12}:Ce^{3+}$ phosphor material used in WLED technology. Wen et al.[119] performed a comprehensive work in which they showed blue, green and red emitting dyes can be incorporated into LMOFs with varying proportion to produce white light with ideal CIE coordinates, high quantum efficiency (upto 26%) and high CRI (upto 92%). The authors used a wide variety of dyes like coumarin derivatives, 4-(dicyanomethylene)-2-methyl-6-(p-dimethylamino styryl)-4H-pyran (DCM) and DSM as blue, green and red emitters inside a MOF, HSB-W1 (HSB = hydrogenated schiff base). The authors claimed that the white light produced via this all-inclusive method is more extensive than the previously reported methods and gave higher quality output. Maji and co-workers[120] showed that sulforhodamine G (SRG) dye molecule can be encapsulated inside the pores of a nano MOF with molecular formula $\{Zn_2(OPE\text{-}TC1)\}_n$ (nMOF-1) where OPE-TC1= oligo-(p-phenylene ethynylene)-based tetracarboxylate – bola-amphiphilic ligand. The resulting MOF, which was a vesicular morphology, resulted in uptake of ambipolar SRG dye. In one of the resulting composites, SRG_2@NMOF-1, with 3.6 mol % SRG loading showed emissions at 472 nm and 562 nm resulting in white light emission with CIE coordinates of (0.31, 0.35). Liu et al.[121] carried out an exemplary work in which they proposed three models viz. a) multiphase single-shell b) single-phase single-shell and c) single-phase multi-shell to construct a series of dye encapsulated MOFs. The MOF chosen was ZIF-8 (ZIF = zeolitic imidazolate framework) which is known for the ease of synthesis in a wide variety of aqueous and non-aqueous solvents, high porosity and structural robustness, and very importantly, the cage like pores, which can effectively trap the dye molecules once they enter the pore space. The dye molecules chosen were rhodamine B or RB (red dye), fluorescein or F (green dye), and 7-amino-4-(trifluoromethyl)-coumarin or C-151 (blue dye) (Figure 12a). Pore-fitting analysis was done to ensure the molecular structure of the dyes was suitable to be incorporated inside the ZIF-8

structure (Figure 12b). In model (a), individual dyes at different wt.% were incorporated inside

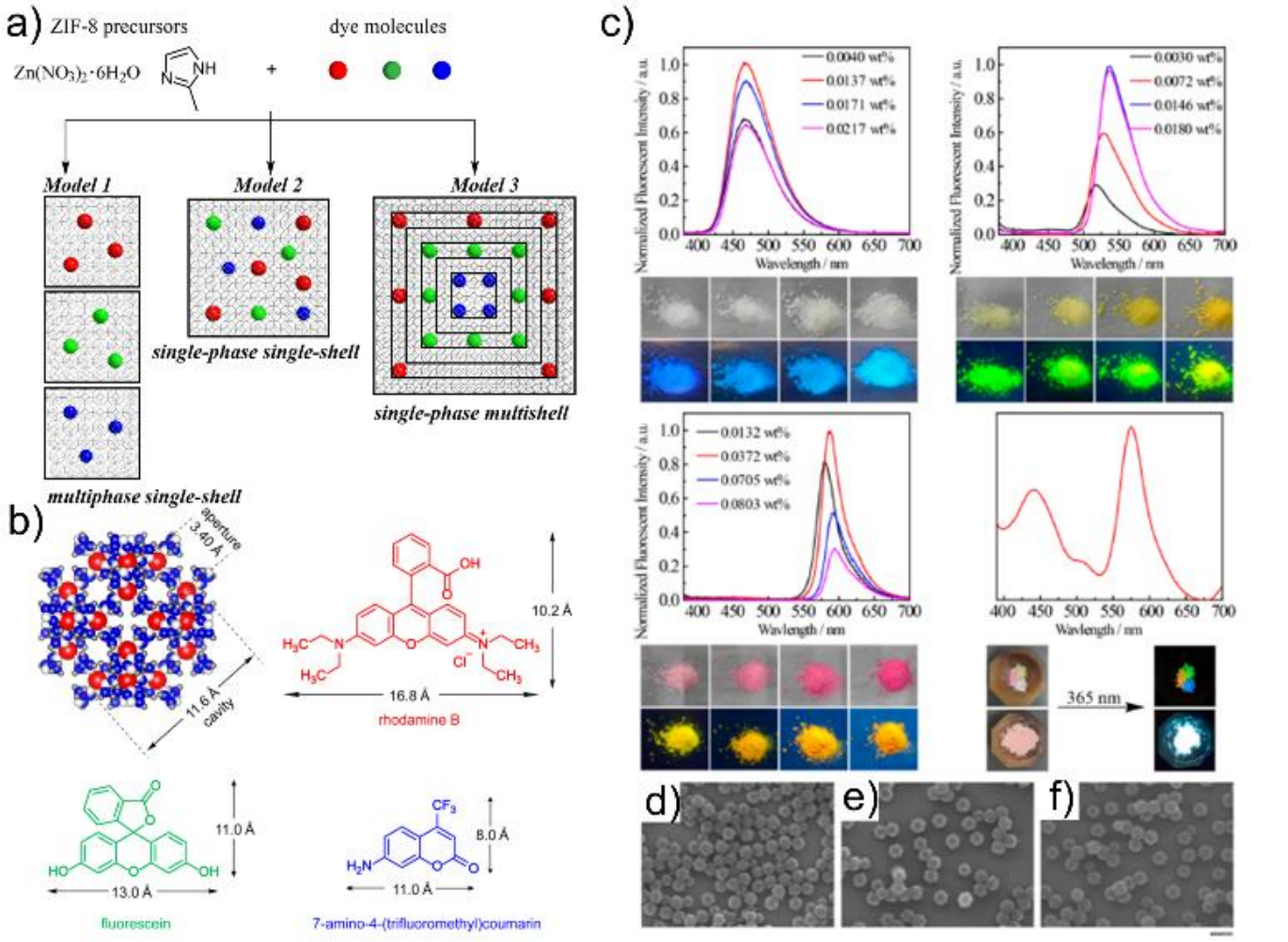

Figure 12: a) Encapsulation of dyes in ZIF-8 by three model approach. b) Molecular dimensions of the dye molecules and pore size of ZIF-8 showing that dyes could fit inside the pores. c) Liquid state fluorescence spectra of C-151@ZIF-8, F@ZIF-8 and RB@ZIF-8, d) SEM images of C-151@ZIF-8, F@ZIF-8, and RB@ZIF-8 showing consistent morphology after dye encapsulation. Reproduced from ref. 121 with permission from American Chemical Society, copyright 2019.

the MOF structure in situ, and the emissions of the composites were checked to confirm successful incorporation of the dye molecules. As expected, the emissions of RB@ZIF-8, C-151@ZIF-8 and F@ZIF-8 showed red, blue and green color respectively with CIE coordinates of (0.57, 0.43), (0.16, 0.12) and (0.26, 0.58) respectively. By varying the ratio of the individual composite and mixing them together appropriately, the authors were able to achieve white light emission with CIE coordinates (0.32, 0.34). The success of model (a) prompted the authors to evaluate model (b), wherein, combining the three dyes inside the nanoporous ZIF-8 structure resulted in the formation of single phase-single shell C-151&F&RB@ZIF-8. However, due to strong fluorescence resonance energy transfer (FRET) occurring between the individual dye molecules inside the pores of the MOF, the efficiency of WLE was significantly reduced. To overcome this drawback, the authors came up with model (c) where dye molecules were encapsulated consecutively via shell-by-shell method. Using this strategy, the color of the dye composites was tuned from pink, yellow and cyan for RB@ZIF-8@C-151@ZIF-8, RB@ZIF-8@F@ZIF-8, and C-151@ZIF-8@F@ZIF-8 respectively keeping the morphology of the composites intact. (Figure 12c, d). As a representative example, C-151@ZIF-8 was chosen as a core for overgrowth of F@ZIF-8 and subsequently RB@ZIF-8. The final CIE coordinates of (0.32, 0.34) were very close to white light which proved that the methodology could be successful in development of phosphor materials for white light. The same team developed an in-situ design strategy[122] to incorporate yellow emitting dyes viz. Rhodamine 6G (R_6G) and 4,9-dibromonaphtho[2,3-

c][1,2,5]thiadiazole (DBNT) inside the pores of two MOFs ZIF-8 and UiO-66 (Figure 13a).

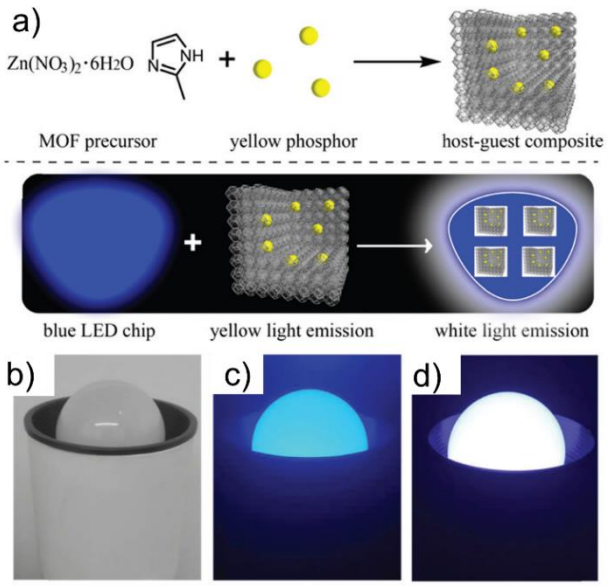

Figure 13: a) Encapsulation of yellow phosphor dyes by in situ approach. b) Blue LED bulb in off state, c) in on state and d) R6G@ZIF-8 coated on the blue LED bulb in on state. Reproduced from ref. 122 with permission from The Royal Society of Chemistry, copyright 2019.

The porous nature and hydrolytic stability of the MOFs chosen were the key features in successful incorporation of the dyes inside the cavities of the MOF. The nanocomposites formed by this method were suitable yellow phosphor materials and could be excitable by yellow light. The R6G@ZIF-8 composite was solution processable and further coated on a blue LED chip to generate pure white light (Figure 13 b-d). QY of 63% was achieved in that case. Their work laid the foundation of a new strategy to encapsulate fluorescent dyes in a myriad of porous MOFs depending on the shape, size and electronic properties of the host-guest entities for high quality white light generation. Cyclodextrin metal–organic frameworks (CD-MOFs) have been known to exhibit high porosity and encapsulate of a wide variety of guest molecules and luminophores inside its cavity.[123] The MOF was used fabricate two composites CD-MOF⊃FL and CD-MOF⊃RhB, based on FL and RhB dye respectively. Very high quantum efficiency of 95% and 82% and green and red-light emissions were observed for CD-MOF⊃FL and CD-MOF⊃RhB respectively. Using the core-shell approach, CD-MOF⊃RhB was selected as the core for the overgrowth of CD-MOF⊃FL (shell) to form a core-shell structure CD-MOF⊃FL@RhB. The luminescent properties of both the core and shell were retained in CD-MOF⊃FL@RhB showing CIE coordinate of (0.45, 0.53). However, one key drawback was a wavelength vacancy of 400 to 500 nm which corresponded to the blue region in the visible spectrum. To address this final piece of puzzle, the authors synthesized a CD-MOF⊃7-HCm (7-HCm=7-hydroxycoumarin). The authors finally designed a near-perfect, visible spectrum encompassing dye composite by choosing CD-MOF⊃FL@RhB as the core shell followed by epitaxial growth of MOF⊃7-HCm to form a new core-shell structure. As a proof of concept, the authors recorded direct emission colors by shinning UV light on the crystals and the luminescent properties were recorded on a camera. Different levels of color were observed in spectrograms and macroscopic photographs which showed that this method could be used for future device fabrication on a commercial scale. More recently, Qian and his group members showed self-assembly of pyrromethene 546 (pm546), pyrromethene 605 (pm605) and sulfurhodamine 101 (SRh101) inside the pores of ZIF-8.[124] To protect the dye@ZIF-8 composites from oxidative degeneration, dye degradation, and fluorescence decay over time, thermoplastic polyurethane (TPU) was coated on the surface as a phosphor layer of the composite materials. After coating, the fluorescence intensity of the pristine phosphor improved significantly (>50%) and the chemical stability issue was also addressed. When the dye composites were coated on a blue LED chip to check white light emission, CIE coordinates of (0.465, 0.413), low CCT of 2642 K and CRI up to 85 were obtained which demonstrates the practical utility of such materials in WLED technology.

Emissive inorganic complexes/QDs incorporation: Another way to achieve multiple emissions in LMOFs is to incorporate transition metal complexes, carbon/perovskite QDs and other emissive inorganic entities.[125, 126] Using the emission properties of such inorganic entities along with the intrinsic emission features of the LMOFs, one can design composites which can generate white light in a much more efficient way. Also, these inorganic components which otherwise face stability issues can be stabilized inside the pores of the MOFs by suitable interactions with the host framework, thus resulting in stable white light generation with much efficient QY. Emissive cationic inorganic complexes can be immobilized in ionic MOFs by facile cation exchange process which has been demonstrated by various groups. Incorporation of such emissive guest molecules inside the porous space of MOFs can result in suitable host-guest interactions which can translate into improving the luminescence output signals including quantum yield, lifetime etc. due to reduced ACQ of such complexes within the confined boundaries of the MOF. Su, Li and co-workers developed an innovative strategy in 2013 to encapsulate a yellow-emitting Ir(III) complex in a blue-emitting MOF.[127] The Ir-based complex chosen was $[Ir(ppy)_2(bpy)]^+$ (Hppy=2-phenylpyridine, bpy=2,2'-bipyridine) which could fit inside the pores of the MOF based on 2,4,6-tris(2,5-dicarboxylphenylamino)-1,3,5-triazine (H_6TATPT) and Cd^{2+}. The resulting MOF with formula $[(CH_3)_2NH_2]_{15}[(Cd_2Cl)_3(TATPT)_4]\cdot 12DMF\cdot 18H_2O$ was a 3D blue emitting MOF with a λ_{max}= 425 nm. The TATPT ligand in free form showed a weak blue emission at 490 nm which was attributed to the π-π* intraligand transition. Upon complexation, in the resulting MOF there was a strong blue shift of 65 nm which the authors corroborated to the MLCT. Once the blue emission of the MOF was established, the authors incorporated $[Ir(ppy)_2(bpy)]^+$ inside the pores of the MOF

(Figure 14a) by cation exchange in DMF solution. Various wt % of the Ir complex loaded MOF composite were synthesized and checked for luminescence behaviour under UV excitation (Figure 14b). At ~7.5 % and 8.8 % loading, the PL spectra for both showed emissions at 425 nm (originating from MLCT in MOF) and 530 nm (originating from $[Ir(ppy)_2(bpy)]^+$). The confinement of the complex in MOF pores resulted in a "rigidochromic effect" which was the reason for such a blue shift in the composites. An optimal loading of 3.5 wt% was found to produce pure white light with CIE coordinates (0.31, 0.33) (Figure 14c), CCT of 5,900 K, and CRI of 80. The broadband emission at such concentration was due to the additive behaviour of the individual components i.e., MOF and the Ir complex. As a proof-of-concept, authors made WLED assemblies based on $[Ir(ppy)_2(bpy)]^+$@MOF by two methods: 1) coating on a commercially available UV LED chip and 2) coating on a InGaAsN chip. The excellent performance of these assemblies in generating white light (Figure 14d) with suitable metrics opened a pandora's box for fabrication of novel WLEDs based on MOF-inorganic guest composites.

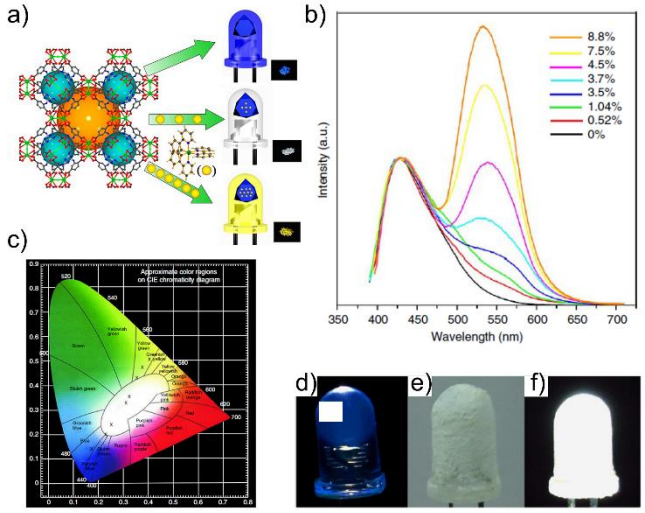

Figure 14: 3D MOF with molecular formula $[(CH_3)_2NH_2]_{15}[(Cd_2Cl)_3(TATPT)_4]\cdot 12DMF\cdot 18H_2O$ showing yellow phosphor properties after encapsulation of Ir-complex. b) PL spectra of the MOF at different % loading of Ir-complex, when excited at 370 nm. c) CIE coordinates of the Ir-complex incorporated MOF. d) Blue LED chip e) MOF coated blue LED chip (off state) and f) MOF coated blue LED chip in on state. Reproduced from ref. 127 with permission from Nature Publishing Group, copyright 2013.

Following this report, several groups have tried to incorporate IR complexes inside the nanocavities of MOFs for WLED application. For example, Zhang et al.[128] reported yellow emitting $[Ir(ppy)_2(bpy)][PF_6]$ encapsulation inside a blue-emitting Zn based LMOF, $[(Zn_4O)(L)(2,6\text{-naphthalic acid})]\cdot 4H_2O\cdot DMF$ (JLNU-7) where H_4L = methanetetra(tetrakis[4-(carboxyphenyl)oxamethyl]-methane acid. The quantum efficiency recorded in this case was 11.9% with CIE coordinates (0.323, 0.298). Xie et al.[129] reported a nanotubular MOF with molecular formula $[(CH_3)_2NH_2]_2[Zn_8(btca)_6(2\text{-}NH_2\text{-}bdc)_3]\cdot 8DMF$ (btca = benzotriazole-5-carboxylic acid and 2-NH_2-bdc=2-amino-1,4-benzenedicarboxylic acid). The resulting blue emitting MOF could act as host material for yellow emitting $[Ir(ppy)_2(bpy)]^+$ complex resulting in the generation of white light with 15.2% quantum yield and CIE coordinates (0.300, 0.336). The composite showed excellent air stability and could generate white light up to a month.

Due to lower cost and more availability, tris(8-hydroxyquinoline) aluminum (Alq_3) could be a suitable replacement for Ir complexes as guest emitters in LMOFs. In 2016, Su and Lan et al. designed a mixed ligand MOF named NENU-521 and encapsulated Alq_3 inside the pores of the MOF.[130] With reduced molecular motions (both vibrational and rotational), the non-radiative decay process of Alq_3 was partially restricted inside the pores of the MOF resulting in quantum yield of 11.4%. The intrinsic yellow-green emission of Alq_3 in combination with the blue emitting MOF resulted in white light emission with CCT value up to 7796 K. However, the composite produced cold white light due to the lack of any suitable red emitter in the composite material.

More recently, QDs have been suitable emitters in MOF pores for white light generation. QDs are known for their high quantum yield, size dependent luminescence and low photo-bleaching.[131] These unique features originate from the quantum confinement effect. Embedding such QDs in porous composites can not only improve their photo-chemical stability but can also carry forward their unique photo-physical properties to the host material like MOFs. Carbon dots (CDs) which have found multifarious applications in photovoltaic devices, LEDs, lithium batteries, have lower toxicity and higher photochemical stability.[132] Taking advantage of these features, Wang et al. [133] and immobilized blue emitting CDs inside the pores of the MOF.[134] The resulting composite showed emission bands at 450 nm and 550 nm originating from CDs and the Zr MOF, when excited at 365 nm. When the authors fabricated WLED based on this composite material, it exhibited down-conversion phosphor properties. The CIE coordinates of (0.31, 0.34) and luminous efficiency of 1.7 lmW^{-1} of the white light produced paved way for the fabrication of CD based REE free composites for SSL applications. Ying et al.[135] presented a "one pot" synthetic method to incorporate red, green and blue (RGB) $CdSexS_{1-x}$/ZnS quantum dots inside the pores of ZIF-8 for fabrication of high efficiency films for WLED applications. The QD@ZIF-8 thin film showed remarkable air and thermal stability and high photo-luminescence quantum yield (PLQY) of 90%. The zinc source for the preparation of ZIF-8 was zinc hydroxide nanostrands (ZHNs). The positive surface charge of ZHNs and the negative QDs resulted in considerable electrostatic interaction between the two components. The RGB-QD@ZIF-8 composite showed bright light illumination (Figure 15) with CIE coordinates (0.33, 0.329), CRI of 90 and CCT of 5600 K and made

a significant advancement in the field of multiple emission centers for WLED applications.

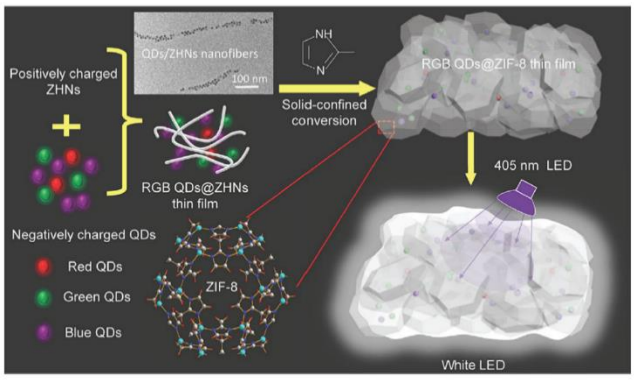

Figure 15: Illustration of $CdSe_xS_{1-x}$/ZnS QDs in ZIF-8 derived from zinc hydroxide nanostrands forming thin film and the corresponding white light emission properties. Reproduced from ref. 135 with permission from John Wiley and Sons, copyright 2017.

Linker functionalization with variable color profiles: Although chromophore installation and immobilization has been a popular strategy to get tunable emission properties, linker functionalization to get full color emission in a single MOF material requires complex and intricate design strategy coupled with reaction engineering. Recently, Li and her group systematically tuned the electronic properties of a UiO-68 based MOF and achieved full color emission.[136] The ligand used in the construction of UiO-68 MOF i.e., [1,1':4',1-terphenyl]-4,4"-dicarboxylic acid (TPDC) was modified at the central core position by 1,3-benzothiadiazole and its analogues (Figure 16a, b). Six different modified ligands were synthesized with varied electronic bandgaps (Figure 16b), and the corresponding MOF materials (Figure 16c, d) viz. UiO-68-BAMB, UiO-68-MBTB, UiO-68-BTMB, and UiO-68-BSMB gave emissions at 445 nm, 470 nm, 520 nm, and 545 nm with high PLQY, whereas for the other two MOFs, UiO-68-NTMB and UiO-68-NSMB gave weaker emissions with low PLQY. The difference in the PL properties was mostly due to ACQ process which is reduced in the first four cases and increased in the latter two due to specific spatial arrangement of the ligands in the MOFs. To improve the PLQY, non-fluorescent linkers were used as a mixed ligand strategy in UiO-68-NTMB and UiO-68-NSMB to significantly reduce the ACQ. This work represented a unique way to achieve tunable color profiles (Figure 16e, f) in LMOFs by linker functionalization approach. In another pioneering work from Li group, five LMOFs HIAM-400X (X=0, 1, 2, 3, 4) based on Zr_6 cluster which had tuneable emissions from blue to red were formulated using 2,1,3-benzothiadiazole and its derivatives (Figures 17 a-c).[137] The terminal OH^-/H_2O of the Zr clusters could be replaced and linker installation (LI) could be successfully achieved. Thirty HIAM-400X-L based MOFs could be synthesized using five HIAM-400X and six second linkers to cover the whole visible spectrum (Figure 17d). Notably, this work was the first example in LMOF literature where two-dimensional space tuning of color was achieved. LI approach can also be used to generate white light as shown by Han et al. [138] The researchers used RGB or yellow-blue emissive organic ligands in an otherwise non fluorescent MOF, NPF-300. The central core responsible for multicolor (MC) emission is the 2,1,3-benzothiadiazole and its analogues which were engineered into the linker resulting in MC-NPF-300-L series MOFs. White light could be generated by a yellow emitting MC-NPF-300-L MOF when excited by blue light. This concept could be extrapolated to other MOFs like PCN-700 as well for WLE. Uribe-Romo et al.[139] proposed a new concept of substitutional solid solution (SSS) and predicted MOFs could be important host matrices for SSS. RGB emissive linkers were installed into non-luminescent MOFs and their emission properties matched to those in their solution phase. The chromaticity coordinates and optical photos revealed high color purity and MC emissions were obtained which mimicked the fluorescence properties of the fluorophore concentration in solution phase. ACQ was reduced due to rigid MOF backbone and the quantum yields were also improved. The authors concluded that SSS materials could find potential applications in SSL technology.

4. Advancement of LMOFs in device fabrication for commercial technology

The potential of LMOFs as REE free phosphors for LED applications has been realized and well documented. However, for the next phase of development, some of these exciting materials needs to be tested in actual devices so that the performances can be evaluated on practical scale and real-time conditions. Although many LMOFs show exciting properties in terms of emission profiles, some other parameters like EQY/IQY, color purity, CCT, must be scrutinized on a comprehensive scale to make LMOFs commercially viable.[140] Moreover, from the material perspective, LMOFs should be highly scalable, robust in terms of physio-chemical stability and photochemical stability so that the technology can be hybridized and brought to market for wide-spread usage. The governing mechanisms while designing LMOF based WLED devices are a) downward conversion and b) electroluminescence (EL). In downward conversion, the electric power is transferred to the blue LED chip/UV chip and the light generated from the chip is generally absorbed by the yellow/white phosphor material (LMOFs for instance) to generate white light. In electroluminescence devices, a thin film OLED is created and electron-hole pair transports through the transport layer and combine in the emission layer to produce white light. As opposed to downward conversion process, this method converts electricity directly into light, thus supposedly giving higher power conversion efficiency. The thickness and roughness of the of the thin films in this case are of paramount importance as charge transport depends on these factors. In this section, we will discuss about some of the LMOFs (both down-converted as EL layers) developed recently which have been tested in devices and can be commercialized. We will briefly touch upon some other hybrid

semiconductor materials based WLED devices too, to give the readers about the advancement in this field for device fabrication.

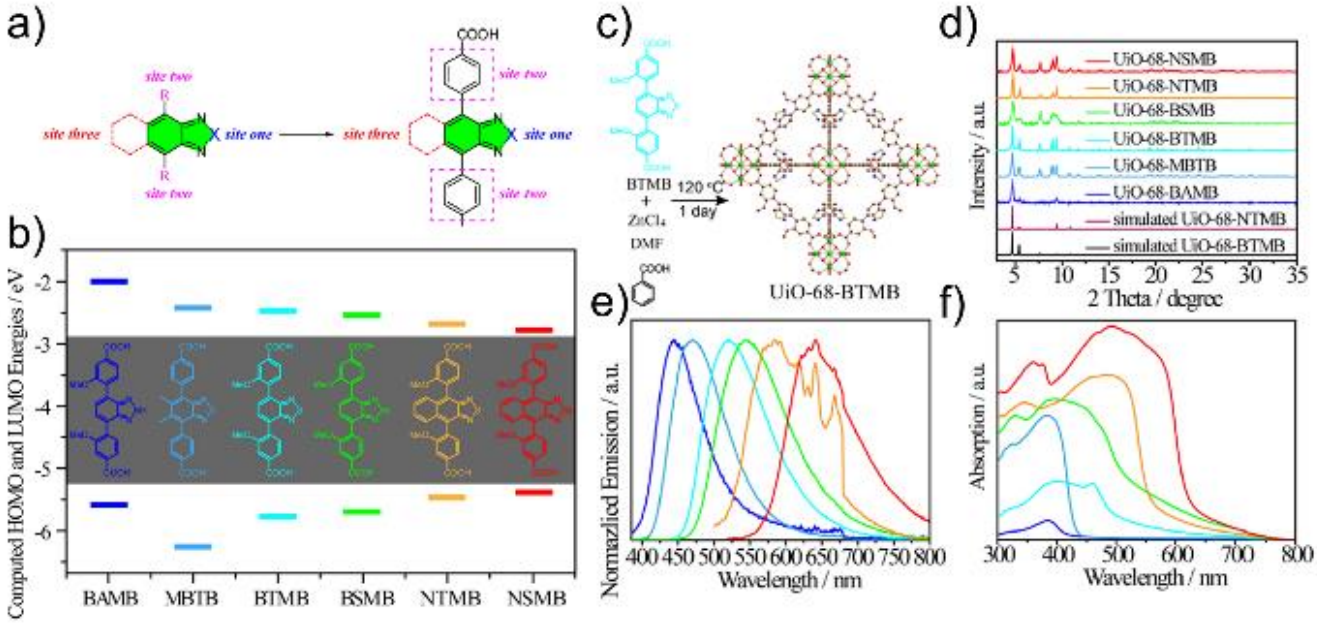

Figure 16: a) Core modification of dicarboxylic acid ligand with 1,3-benzothiadiazole and its analogues. b) HOMO-LUMO energy gap of six different core-modified ligands used for the UiO-68 based MOF structures. c) Synthetic scheme of UiO-68-BTMB MOF. d) Powder x-ray diffraction patterns of six MOFs showing isostructural nature. e) Emission spectra and UV-vis spectra of UV−vis absorption spectra of UiO-68-BAMB, UiO-68-MBTB, UiO-68-BTMB, UiO-68-BSMB, UiO-68-NTMB, and UiO-68-NSMB. Reproduced from ref. 136 with permission from The American Chemical Society, copyright 2021.

A list of LMOFs discussed in this article along with the mechanism underlying their emission, photophysical properties and key metrics for device implementation is summarized in Table 1. Recently Chaudhari et al.[141] documented a "high concentration reaction" (HCR) based approach for one-pot fabrication of guest encapsulated nano MOF in high yield. Simultaneous nanoconfinement of two fluorophore dye molecules viz. a) fluorescein and b) rhodamine in the pores of ZIF-8 resulting in "dual-guest" hybrid material, A+B@ZIF-8 (Figures 18 a, b). The composite material showed yellow emission at 511 nm and could be further combined with a blue emitting polymer resin which could be 3D printed using stereolithography technique. The QY of A+B@ZIF-8 solid was found to be 47.3% and that of the 3D printed pellets were found to be 43.6%. The WLE of these 3D printable objects with 3 mm thickness were further carried out, to put forward the practical usage of these engineered objects for future device implementation (Figures 18 c-h). Guest@MOF for EL layer in devices was further demonstrated by Gutiérrez et al.[142] Using the same HCR approach, the authors encapsulated gallium(III) tris(8-hydroxyquinolinato) (Gaq_3) in ZIF-8 to make Gaq_3@ZIF-8. The authors used this material for white light generation via both down-conversion and EL methods. In the first process, nanoparticles of Gaq3@ZIF-8 were dispersed in a polymer and a 405 nm LED was coated onto it. The combination of blue and yellow light resulted in down-converted uniform white light emission. In the second method, Gaq3@ZIF-8 composite was used as an EL layer in a multilayer device showing I-V characteristics of LED with a bias voltage of 3V, emitting broadband spectrum. Interestingly, by dispersing the EL particles in a polymer matrix (CN-PPV) the bias voltage was reduced by half and the quantum efficiency was improved. Mondal et al.[143] fabricated a LED device which emitted high intensity white light at different bias voltages. A Zn based MOF ($ZnipaPy_2$), was used an active emissive layer which generated white light with CIE coordinates of (0.31, 0.33) and quantum yield of 32.5%. To construct the device, a hole conducting layer poly[3,4-(ethylenedioxy)thiophene]:poly-(styrenesulfonate) (PEDOT:PSS) was coated on a indium tin oxide-coated glass substrate. Then the MOF solution which was the active emissive layer was spin coated over the PEDOT:PSS layer followed by thermal evaporation of the electron conducting layer of (8-hydroxyquinolinato)aluminum (Alq_3). The stability of the device was found to be 20-25 minutes and the luminescence was consistent up to 3 days. The device (ITO/PEDOT:PSS/$ZnipaPy_2$/Alq_3/Al) showed three EL peaks at 445 nm, 537 nm and 602 nm and cover the whole range of visible spectrum. The authors performed DFT calculations and predicted the electron and hole transport mechanism occurring in the device. This research provided a nice addition to the advancement of single component LMOF based material for device implementation. Gong et al.[84] designed a prototype WLED device based on the previously discussed MOF, $[Zn_6(btc)_4(tppe)_2(DMA)_2]$. The MOF was coated on a 5mm blue LED bulb. The coating suspension was prepared in ethyl acetate followed by sonication. Then an ultrathin film was coated on the bulb and the device generated white light at 3V bias with a luminous efficiency of 47.4 lm/W which was much higher than the requirement for small-sized LED bulbs. A relatively high QY yellow

phosphor Ca-MOF developed by Li group could be coated on a commercial blue LED chip and generated bright white light devices (Figures 19 a-c).[88] At that time, it was the first report of alkaline earth metal based LMOFs for LED

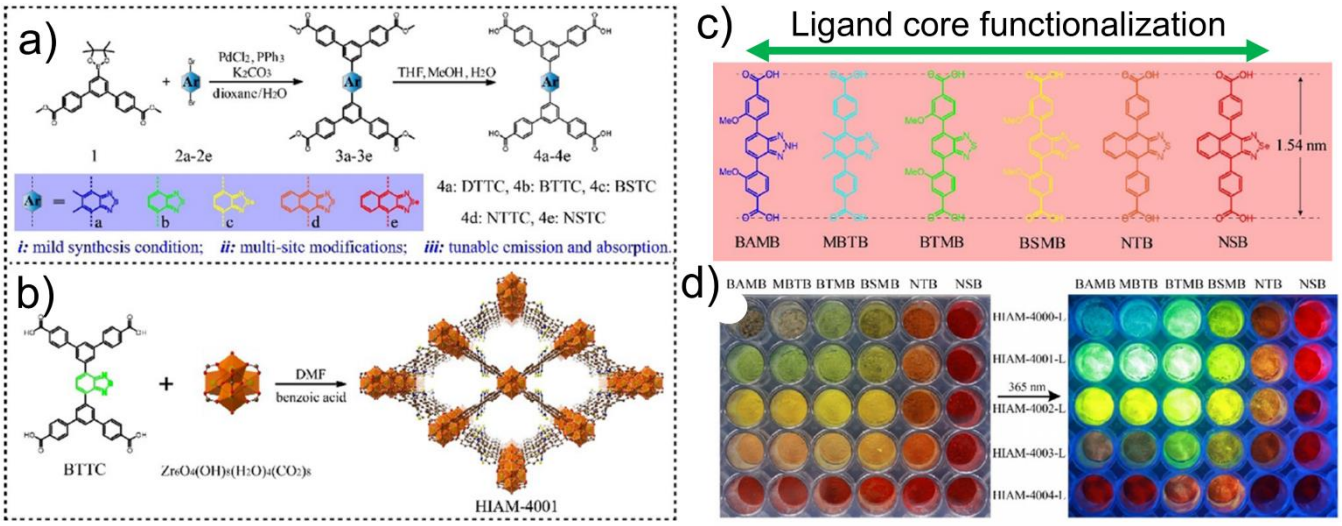

Figure 17: a) Synthesis scheme of 2,1,3-benzothiadiazole and its analogues modified tetracarboxylic acid ligand. b) Synthesis of HIAM-401 from BTTC ligand. c) Five different core modified ligands used for MOF synthesis. d) Photographs of thirty different HIAM-400X-L MOFs based on five ligands and six co-ligands showing full range of color in the visible spectrum when excited by 365 nm UV light. Reproduced from ref. 137 with permission from John Wiley and Sons, copyright 2021.

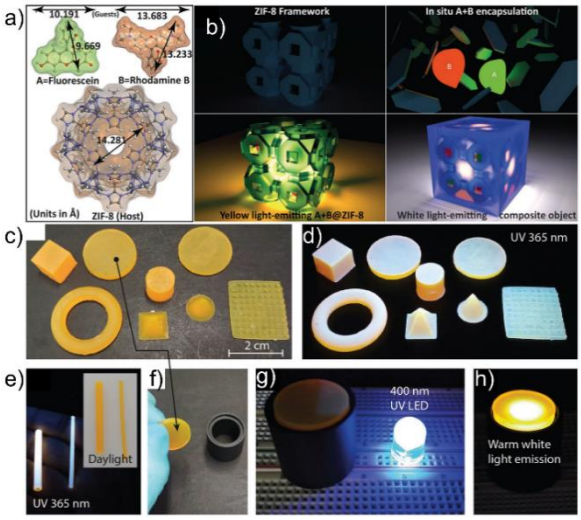

Figure 18: a) Molecular structure and size of dye molecules and comparison with the pore size of ZIF-8. b) A+B@ZIF-8 resulting in white light generation by combing with blue photopolymer resin. c), d) 3D printed composite materials showing white light under UV light. e-f) Pellets in disc shaped support to produce warm white light upon UV excitation at 400 nm. Reproduced from ref. 144 with permission from John Wiley and Sons, copyright 2020.

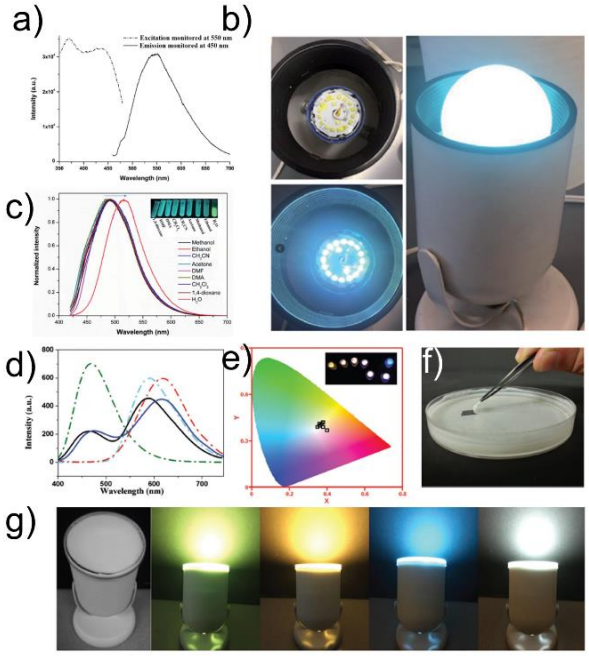

Figure 19: a)-c) WLED device based on yellow phosphor [Ca_4(tcbpe-F)$_2$(H_2O)$_3$]. Reproduced from ref. 90 with permission from The Royal Society Chemistry, copyright 2022. d) Tunable luminescence profile of Cu_4I_4 based hybrid structures with N-donor ligands. e) CIE coordinates of the blue and white phosphor composites. f) device performance after coating with the binder showing tunable light generation depending on the nature of the composites. Reproduced

from ref. 144 with permission from The John Wiley and Sons, copyright 2017.

device application. Some other inorganic-organic crystalline hybrid materials developed in Li group have also shown promising potential in LED devices. For example, in 2017, her group fabricated Cu_4I_4 based 1D, 2D and 3D hybrid materials in association with a wide variety of N-donor ligands [144]. The resulting materials showed bright yellow-orange emission with a QY ranging from 56%-96%. Since the phosphor materials were solution processable, the authors designed a prototype device where a white phosphor among the synthesized materials along with a water-soluble binder PolyOx N-750, were mixed in ethanol followed by evaporation, to give a thin resin film. The layer was coated onto the inner surface of a UV light bulb to prevent direct contact. The layer could be removed as a uniform thin film from the surface thus validating the fabrication and coating process. The prototype device produced warm white light stable for weeks.

5. Futuristic outlook and conclusion

In this feature article, we have given a brief overview of the recent progress of LMOFs as environmentally favorable phosphor materials for energy-saving SSL technology. Representative work (including our own) on REE-free LMOFs for WLED applications has been discussed and the potential of these fascinating materials in device implementation has been assessed. We have also briefly outlined various emission mechanisms which are governed by multiple units including metal, ligands, and guest species. Host-guest chemistry, AIE, dye encapsulation, ion-exchange, emissive inorganic component installation and chromophore immobilization are some of the key parameters/factors while designing suitable phosphor materials. These unique features make LMOFs as forerunners in future "greener" materials to be used in LED industry. The usage of REE-based materials is undesirable because of limited resources and environmental concerns. Also, from the global energy consumption standpoint, materials which can give highest energy output are always desired. LMOFs have crossed the first barrier in terms of promising potential and possible hybridization technology. Moving forward, several unanswered questions have to be addressed: 1) Economics: The cost of MOFs is generally high. Barring a few building units that are used for MOF synthesis, the majority of the organic ligands and metal salts are cost intensive. Therefore, research must be directed towards developing less expensive MOF materials which can be made in bulk scale and fit to be used in widespread commercial purposes. For this, academia and industry must join hands to come up with breakthrough solutions in material design and cost effectiveness. 2) Chemical stability: Since LMOFs are often made up of transition metal ions, they are susceptible to hydrolysis or lack chemical stability. To address this issue, robust SBUs with high valence metal ions and chemically resistant organic struts with strong metal-ligand bonds must be used which impart physio-chemical stability over long periods. Zr-based MOFs have proven to be such highly stable frameworks. Blue-emitting Zr-MOFs have thus found promising applications in various opto-electronic applications. Also, chemical modification in some MOFs improves the water/air stability, which makes post-synthetic modification an effective tool to improve chemical stability. 3) QY: The emission efficiency directly impacts the future of LMOFs for device implementation and commercialization. Some orange and red emitting phosphor materials have low quantum yield which restricts their usage in lighting devices. Use of chromophoric ligands from red-emitting organic precursors can reduce the non-radiative decay once installed in the backbone of REE-free MOFs, and thus greatly enhance the QY.

Table 1. List of selected LMOFs and summary of their emission characteristics, mechanisms and device performance properties (if any) for WLEDs.

MOF	Excitation Wavelength(nm)	Emission Color	Mechanism	Device Characteristics (IQY/CCT/CRI/CIE coordinates etc.)	Reference
$[Zn_6(btc)_4(tppe)_2(DMA)_2]\cdot 9DMA\cdot 12H_2O$	400	Yellow	AIE	IQY = 90.7% CIE coordinates (0.39, 0.57)	[84]
LMOF-231 LMOF-241 LMOF-305	365 (LMOF-231) 340 (LMOF-241) 455 (LOMOF-305)	Yellow	AIE	IQY = 95.1% IQY = 92.7% IQY = 88%	[85]
LMOF-263	455	Yellow	AIE	IQY = 42.5%	[87]
LMOF-301	455	Yellow	AIE	IQY = 50.9%	

[Ca(H_2tcbpe-F)(H_2O)$_2$]	450	Yellow	AIE	IQY = 68% CIE coordinates (0.39, 0.55)	[90]
[Zn(tppa)(ndc)·(DMF)$_4$] Zn_4(tppa)$_2$(sdc)$_3$(NO_3)$_2$·(DMF)$_4$·(ACN)$_2$	455 455	Yellow Yellow	AIE	11.4% 20.6%	[91]
bio-MOF-101-BCPPE	375	Green-Yellow	AIE	IQY = 42% CIE (0.35,0.36)	[92]
(Zr-TCBPE-MOL)	450	Yellow	AIE	IQY = 50% CIE coordinates (0.42, 0.54)	[93]
[AgL]$_n$·nH_2O	355	Yellow	CT	IQY = 10% CIE coordinates (0.31, 0.33)	[97]
[MgL_2(H_2O)$_2$]·3.5H_2O [MgL_2(DMF)$_2$]·3.5H_2O [MgL_2(DEF)(H_2O)]·3H_2O	468	Yellow Yellow Yellowish orange	CT	IQY = 14.6% IQY = 18.1% IQY = 2.4%	[98]
TJU-6 TJU-7	360 370	White	CT	IQY = 5.6% IQY = 1.8% CCT = 5727 K	[99]
Pb(HL_3)(1,4-dioxane)$_{0.5}$ Pb_2(HL_3)$_2$(H_2O)$_5$	350 350	Greenish yellow White	ILCT, MLCT, LMCT	CIE coordinates (0.34, 0.44) CIE coordinates (0.33, 0.36)	[99]
{(Pb_4Cl_2)(ndc)$_4$·[(CH_3)$_3$NH]$_2$}$_n$ [(Pb_4Br_2)(ndc)$_4$·{(CH_3)$_2$$NH_2$]$_2$}$_n$ {(Pb_4I_2)(ndc)$_4$·[(CH_3)$_2$NH]$_2$}$_n$	365	Blue White White	LMCT	6.1%, (0.2512, 0.2231) 11.9%, (0.3455, 0.2947) 9.7%, (0.3339, 0.2831)	[101]
TMOF-5(X) (X = Cl/Br/I)	367 380 422	White White White	CT	CCT = 4784K, CRI = 85, CIE coordinates (0.36, 0.40), EQY= 6-8 % (Cl analogue) CCT = 4258K, CRI = 89, CIE coordinates (0.37,0.39), EQY= 1.5 % (Br analogue) CCT = 3972, CRI = 70, CIE	[102]

				coordinates (0.40, 0.48) (I analogue)	
$[Sr(Hbtc)(H_2O)]_n$	266	White	LMCT	Eg = 2.3 eV	[104]
(TBA)[$BiBr_4$(bp4mo)] [$BiBr_3$(bp4mo)$_2$]	409	Yellow	CT, Aggregation-induced phosphores-cence	IQY = 85% IQY = 11%	[105]
$[Cd(tzphtpy)_2]_n$·6.5n H_2O	326	Yellow	LLCT	CCT = 5328 K, PLQY = 2.3%, CIE coordinates (0.33, 0.36)	[106]
ZJU-28⊃DSM/AF	365	White	Dye encapsulation	CCT = 5327 K, CRI = 91 QY = 17.4%, CIE coordinates (0.34, 0.32)	[117]
RhB@Al-DBA	395	White	Dye encapsulation	CCT = 6085 K, QY = 12%, CIE coordinates (0.32, 0.30), Power density = 0.89 mW/cm^2 in WL assembly.	[118]
HSB-W1⊃DCM/C6/CBS-127	365	White	Multiple dye encapsulation	CCT = 5533 K, CRI = 80, QY = 20.2%, CIE coordinates (0.33, 0.32)	[119]
$\{Zn_2(OPE\text{-}TC1)\}_n$	376	White	Dye encapsulation	CIE coordinates (0.31, 0.35)	[120]
C151@ZIF-82@F@ZIF-82@RB@ZIF-8	365	White	Multiple dye encapsulation	CIE coordinates (0.32, 0.34)	[121]
R6G@ZIF-8 DBNT@UiO-66	365-420	Yellow	Dye encapsulation	QY = 34.5% QY = 22.7%	[122]
CD-MOF⊃7-HC_m@FL@RhB	365	White	Multiple dye encapsulation	CIE coordinates (0.35, 0.32)	[123]
ZIF-8⊃pm546/pm605/SRh101	460	White	Dye encapsulation	CIE coordinates (0.465, 0.413) QY = 66.3%CCT = 2642 K CRI = 85	[124]
$[Ir(ppy)_2(bpy)]^+$@ $[(CH_3)2NH_2]_{15}[(Cd_2Cl)_3(TATPT)_4]$	370	White	Emissive inorganic complex encapsulation; π-π* intraligand transition, MLCT	CIE coordinates (0.31, 0.33) CCT = 5,900 K, CRI = 80	[127]
$[Ir(ppy)_2(bpy)][PF_6]$ @JLNU-7	380	White	Emissive inorganic complex encapsulation; π-	QY = 11.9%, CIE coordinates (0.323, 0.298)	[128]

			π* intraligand transition, MLCT		
$[Ir(ppy)_2(bpy)]^+$@ NENU-524	370	White	Emissive inorganic complex encapsulation; π-π* intraligand transition, MLCT	QY = 15.2%, CIE coordinates (0.300, 0.336	[129]
Alq_3@NENU-521	370	White	Emissive inorganic complex encapsulation; π-π* intraligand	CIE coordinates (0.291, 0.327) QY up to 11.4%	[130]
CDs/Zr-MOF	365	White	Emissive inorganic complex encapsulation	CIE coordinates (0.31, 0.34), QY = 37%, CRI = 82, luminous efficiency of 1.7 lm W^{-1}	[125]
$CdSe_xS_{1-x}$ /ZnS @ ZIF-8	405	White	Emissive inorganic complex encapsulation	CIE coordinates (0.33, 0.329), CRI = 90 and CCT = 5600 K	[135]
UiO-68-BAMB, UiO-68-MBTB, UiO-68-BTMB, and UiO-68-BSMB, UiO-68-NTMB and UiO-68-NSMB	365	Full color	Linker installation for full color emission	QY = 5.80% (UiO-68-BAMB), 14.6% (UiO-68-MBTB), 36.0% (UiO-68-MBTB), 2.80% (UiO-68-NTMB) 0.30% (UiO-68-BSMB) 0.70% (UiO-68-NSMB)	[136]
HIAM-400X	365	Full color emission	Linker installation	QY = 21.1%, 44.0%, 28.4%, 17.6% and 7.70% for HIAM-4001-4004 respectively	[137]
A+B@ZIF-8	365	White	Dye encapsulation	CIE coordinates (0.1888,0.1114), CCT = 3700 K, QY = 43-46%	[141]
Gaq_3@ZIF-8	365	green-yellow	Emissive inorganic complex encapsulation	CIE coordinates (0.27, 0.34), QY = 15%, bias voltage = 3V	[142]

This could also have a direct effect on the cost of the phosphor materials as the current red emitting LMOFs are mostly based on expensive Eu (III) ions. 4) Photobleaching and leaching: For longer lifetime and stability, LMOFs which have strong emitting guests such as dye molecules and inorganic complexes must possess good photostability and low leaching. This can be achieved by choosing photochemically stable guest species and those that can be held by strong host-guest interaction inside the MOF framework. Organic dyes with highly conjugated structures can undergo suitable electronic interactions with the MOF framework and can overcome the problem of leaching. From device engineering perspective, several other factors such as solution processability, flexibility, binder-free approach must also be taken into consideration from the context of real-world applications.

Undoubtedly, LMOFs hold unprecedented potential as REE-free alternate phosphor materials. But quoting John Frost “And miles to go before I sleep” - MOF researchers have to traverse through a long tunnel to see LMOFs being finally implemented as a viable alternative to the lighting technology. We are hopeful that this feature article

will encourage scientists across all domains to work as a unified force to realize the dream of a green WLED technology for the future.

Conflicts of interest

No conflict of interest is declared.

Acknowledgements

JL acknowledge the partial support from the U.S. Department of Energy (grant number DE-SC0019902).

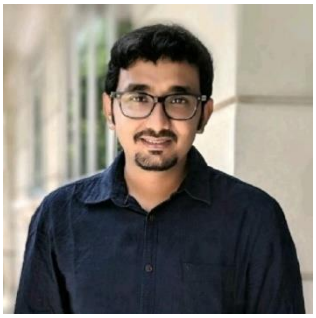

Avishek Karmakar did his BS and MS from University of Calcutta and University of Delhi respectively. He then pursued his PhD from Indian Institute of Science, Education and Research (IISER) Pune and completed it in 2017. His PhD research was on development of luminescent MOFs for anion recognition and sequestration. He did his postdoctoral training at the National University of Singapore where he worked extensively on stimuli responsive MOFs for water-based applications. His overall research interest is on MOFs and other crystalline materials for key applications related to energy and environment. He also serves as independent reviewer and editor for various journals.

Jing Li is a Distinguished Professor in the Department of Chemistry and Chemical Biology at Rutgers University, USA. She received her PhD degree from Cornell University in 1990 under the guidance of Professor Roald Hoffmann. She joined the chemistry faculty at Rutgers University in 1991 as Assistant Professor. She was promoted to Associate Professor in 1996, to full Professor in 1999, and to Distinguished Professor in 2006. She has published 410+ research articles, invited book chapters and reviews, and holds 15 issued and pending patents. Her research focuses on the development of functional materials for renewable, sustainable and clean energy related applications.

Notes and references

‡ Footnotes relating to the main text should appear here. These might include comments relevant to but not central to the matter under discussion, limited experimental and spectral data, and crystallographic data.

1. L. T. Doulos, A. Kontadakis, E. N. Madias, M. Sinou and A. Tsangrassoulis, *Energy and Buildings*, 2019, **194**, 201-217.
2. C. Dortans, M. W. Jack, B. Anderson and J. Stephenson, *Energy Efficiency*, 2020, **13**, 1105-1118.
3. Y. Hou, *AIP Conference Proceedings*, 2018, **1971**, 040018.
4. C. J. Andrews and U. Krogmann, *Energy Policy*, 2009, **37**, 541-553.
5. O. Ilic, P. Bermel, G. Chen, J. D. Joannopoulos, I. Celanovic and M. Soljačić, *Nature Nanotechnology*, 2016, **11**, 320-324.
6. D. H. Sliney, *Eye*, 2016, **30**, 222-229.
7. P. E. Hartman and W. H. Biggley, *Environmental and Molecular Mutagenesis*, 1996, **27**, 306-313.
8. D. A. Steigerwald, J. C. Bhat, D. Collins, R. M. Fletcher, M. O. Holcomb, M. J. Ludowise, P. S. Martin and S. L. Rudaz, *IEEE Journal of Selected Topics in Quantum Electronics*, 2002, **8**, 310-320.
9. I. L. Azevedo, M. G. Morgan and F. Morgan, *Proceedings of the IEEE*, 2009, **97**, 481-510.
10. J. Y. Tsao, M. H. Crawford, M. E. Coltrin, A. J. Fischer, D. D. Koleske, G. S. Subramania, G. T. Wang, J. J. Wierer and R. F. Karlicek Jr., *Advanced Optical Materials*, 2014, **2**, 809-836.
11. E. F. Schubert and J. K. Kim, *Science*, 2005, **308**, 1274-1278.
12. A. De Almeida, B. Santos, B. Paolo and M. Quicheron, *Renewable and Sustainable Energy Reviews*, 2014, **34**, 30-48.
13. P. Pattison, s. bland, n. bardsley and L. Pattison, *Solid-State Lighting Research and Development Multi-Year Program Plan*, 2014.
14. M. G. Craford, *LEDs for solid state lighting and other emerging applications: status, trends, and challenges*, SPIE, 2005.
15. Y. Narukawa, M. Ichikawa, D. Sanga, M. Sano and T. Mukai, *Journal of Physics D: Applied Physics*, 2010, **43**, 354002.
16. Z. Wu and Z. Xia, in *Nitride Semiconductor Light-Emitting Diodes (LEDs) (Second Edition)*, eds. J. Huang, H.-C. Kuo and S.-C. Shen, Woodhead Publishing, 2018, DOI: https://doi.org/10.1016/B978-0-08-101942-9.00005-8, pp. 123-208.
17. R.-J. Xie and N. Hirosaki, *Science and Technology of Advanced Materials*, 2007, **8**, 588-600.
18. K. Panigrahi and A. Nag, *The Journal of Physical Chemistry C*, 2022, **126**, 8553-8564.
19. Y. N. Ahn, K. D. Kim, G. Anoop, G. S. Kim and J. S. Yoo, *Scientific Reports*, 2019, **9**, 16848.
20. S. Ye, F. Xiao, Y. X. Pan, Y. Y. Ma and Q. Y. Zhang, *Materials Science and Engineering: R: Reports*, 2010, **71**, 1-34.
21. R. G. Davis and D. N. Ginthner, *Journal of the Illuminating Engineering Society*, 1990, **19**, 27-38.
22. A. R. Robertson, *Color Research & Application*, 1977, **2**, 7-11.
23. C. R. Ronda, T. Jüstel and H. Nikol, *Journal of Alloys and Compounds*, 1998, **275-277**, 669-676.
24. R. P. Rao and D. J. Devine, *Journal of Luminescence*, 2000, **87-89**, 1260-1263.
25. M. Zhao, Q. Zhang and Z. Xia, *Accounts of Materials Research*, 2020, **1**, 137-145.
26. D. Ravichandran, R. Roy, W. B. White and S. Erdei, *Journal of Materials Research*, 1997, **12**, 819-824.
27. D. Kim, *Nanomaterials*, 2021, **11**.
28. K. M. Goodenough, F. Wall and D. Merriman, *Natural Resources Research*, 2018, **27**, 201-216.
29. D. Alezi, Y. Belmabkhout, M. Suyetin, P. M. Bhatt, Ł. J. Weseliński, V. Solovyeva, K. Adil, I. Spanopoulos, P. N. Trikalitis, A.-H. Emwas and M. Eddaoudi, *Journal of the American Chemical Society*, 2015, **137**, 13308-13318.
30. S. Ma and H.-C. Zhou, *Chemical Communications*, 2010, **46**, 44-53.
31. L. Zhu, X.-Q. Liu, H.-L. Jiang and L.-B. Sun, *Chemical Reviews*, 2017, **117**, 8129-8176.
32. I. Abánades Lázaro and R. S. Forgan, *Coordination Chemistry Reviews*, 2019, **380**, 230-259.
33. X. Zhang, A. Chen, M. Zhong, Z. Zhang, X. Zhang, Z. Zhou and X.-H. Bu, *Electrochemical Energy Reviews*, 2019, **2**, 29-104.
34. Z. Hu, B. J. Deibert and J. Li, *Chemical Society Reviews*, 2014, **43**, 5815-5840.
35. W. P. Lustig, S. Mukherjee, N. D. Rudd, A. V. Desai, J. Li and S. K. Ghosh, *Chemical Society Reviews*, 2017, **46**, 3242-3285.
36. Y. Tang, H. Wu, W. Cao, Y. Cui and G. Qian, *Advanced Optical Materials*, 2021, **9**, 2001817.
37. H. Kaur, S. Sundriyal, V. Pachauri, S. Ingebrandt, K.-H. Kim, A. L. Sharma and A. Deep, *Coordination Chemistry Reviews*, 2019, **401**, 213077.

38. R. Medishetty, J. K. Zaręba, D. Mayer, M. Samoć and R. A. Fischer, *Chemical Society Reviews*, 2017, **46**, 4976-5004.
39. Y. Cui, J. Zhang, H. He and G. Qian, *Chemical Society Reviews*, 2018, **47**, 5740-5785.
40. X.-Y. Liu, W. P. Lustig and J. Li, *ACS Energy Letters*, 2020, **5**, 2671-2680.
41. S. Jensen, K. Tan, W. P. Lustig, D. S. Kilin, J. Li, Y. J. Chabal and T. Thonhauser, *Chemistry of Materials*, 2019, **31**, 7933-7940.
42. M. Rubio-Martinez, C. Avci-Camur, A. W. Thornton, I. Imaz, D. Maspoch and M. R. Hill, *Chemical Society Reviews*, 2017, **46**, 3453-3480.
43. D. Zhao, D. J. Timmons, D. Yuan and H.-C. Zhou, *Accounts of Chemical Research*, 2011, **44**, 123-133.
44. Y. Cui, Y. Yue, G. Qian and B. Chen, *Chemical Reviews*, 2012, **112**, 1126-1162.
45. Y. Cui, B. Chen and G. Qian, *Coordination Chemistry Reviews*, 2014, **273-274**, 76-86.
46. H.-Y. Li, S.-N. Zhao, S.-Q. Zang and J. Li, *Chemical Society Reviews*, 2020, **49**, 6364-6401.
47. W. Liu, W. P. Lustig and J. Li, *EnergyChem*, 2019, **1**, 100008.
48. S. Parola, B. Julián-López, L. D. Carlos and C. Sanchez, *Advanced Functional Materials*, 2016, **26**, 6506-6544.
49. J. Chen, H. Xiang, J. Wang, R. Wang, Y. Li, Q. Shan, X. Xu, Y. Dong, C. Wei and H. Zeng, *ACS Nano*, 2021, **15**, 17150-17174.
50. T. Guner and M. M. Demir, *physica status solidi (a)*, 2018, **215**, 1800120.
51. X. Li, M. Rui, J. Song, Z. Shen and H. Zeng, *Advanced Functional Materials*, 2015, **25**, 4929-4947.
52. T. N. Nguyen, F. M. Ebrahim and K. C. Stylianou, *Coordination Chemistry Reviews*, 2018, **377**, 259-306.
53. N. U. Islam, M. Usman, S. Rasheed and T. Jamil, *ECS Journal of Solid State Science and Technology*, 2021, **10**, 106004.
54. Q. Mo, Y. Shi, W. Cai, S. Zhao, Y. Ying and Z. Zang, *Journal of Physics D: Applied Physics*, 2022, **55**, 333003.
55. L. Wang, J. Cui, Q. Shi, Y. Tian, C. e. Cui, M. Ren and P. Huang, *Journal of Alloys and Compounds*, 2018, **764**, 1003-1007.
56. K. Van den Eeckhout, P. F. Smet and D. Poelman, *Materials*, 2010, **3**, 2536-2566.
57. V. Awate, R. Tiwari, A. K. Shrivastava, N. Dubey and V. Dubey, *Journal of Materials Science: Materials in Electronics*, 2018, **29**, 4391-4401.
58. K. Uheda, N. Hirosaki, Y. Yamamoto, A. Naito, T. Nakajima and H. Yamamoto, *Electrochemical and Solid-State Letters*, 2006, **9**, H22.
59. T. Wu, C.-W. Sher, Y. Lin, C.-F. Lee, S. Liang, Y. Lu, S.-W. Huang Chen, W. Guo, H.-C. Kuo and Z. Chen, *Applied Sciences*, 2018, **8**, 1557.
60. V. Wood and V. Bulović, *Nano Reviews*, 2010, **1**, 5202.
61. A. Karmakar, P. Samanta, S. Dutta and S. K. Ghosh, *Chemistry – An Asian Journal*, 2019, **14**, 4506-4519.
62. A. Karmakar, P. Samanta, A. V. Desai and S. K. Ghosh, *Accounts of Chemical Research*, 2017, **50**, 2457-2469.
63. W. Xie, S.-R. Zhang, D.-Y. Du, J.-S. Qin, S.-J. Bao, J. Li, Z.-M. Su, W.-W. He, Q. Fu and Y.-Q. Lan, *Inorganic Chemistry*, 2015, **54**, 3290-3296.
64. B. J. Deibert, E. Velasco, W. Liu, S. J. Teat, W. P. Lustig and J. Li, *Crystal Growth & Design*, 2016, **16**, 4178-4182.
65. L. Ai, Y. Yang, B. Wang, J. Chang, Z. Tang, B. Yang and S. Lu, *Science Bulletin*, 2021, **66**, 839-856.
66. K.-L. Wong, J.-C. G. Bünzli and P. A. Tanner, *Journal of Luminescence*, 2020, **224**, 117256.
67. W. P. Lustig and J. Li, *Coordination Chemistry Reviews*, 2018, **373**, 116-147.
68. Y. Liu, X.-Y. Xie, C. Cheng, Z.-S. Shao and H.-S. Wang, *Journal of Materials Chemistry C*, 2019, **7**, 10743-10763.
69. M. Pan, W.-M. Liao, S.-Y. Yin, S.-S. Sun and C.-Y. Su, *Chemical Reviews*, 2018, **118**, 8889-8935.
70. J. Heine and K. Müller-Buschbaum, *Chemical Society Reviews*, 2013, **42**, 9232-9242.
71. T. Mehmood and J. P. Reddy, in *Progress in Molecular Biology and Translational Science*, eds. R. S. Bhosale and V. Singh, Academic Press, 2021, vol. 185, pp. 179-198.
72. G.-L. Yang, X.-L. Jiang, H. Xu and B. Zhao, *Small*, 2021, **17**, 2005327.
73. A. Karmakar, E. Velasco and J. Li, *National Science Review*, 2022, DOI: 10.1093/nsr/nwac091.
74. P. Samanta, S. Let, W. Mandal, S. Dutta and S. K. Ghosh, *Inorganic Chemistry Frontiers*, 2020, **7**, 1801-1821.
75. B.-B. Guo, J.-C. Yin, N. Li, Z.-X. Fu, X. Han, J. Xu and X.-H. Bu, *Advanced Optical Materials*, 2021, **9**, 2100283.
76. L. Giri, S. R. Rout, R. S. Varma, M. Otyepka, K. Jayaramulu and R. Dandela, *Nanotechnology Reviews*, 2022, **11**, 1947-1976.
77. G. A. Leith, C. R. Martin, J. M. Mayers, P. Kittikhunnatham, R. W. Larsen and N. B. Shustova, *Chemical Society Reviews*, 2021, **50**, 4382-4410.
78. A. M. Rice, C. R. Martin, V. A. Galitskiy, A. A. Berseneva, G. A. Leith and N. B. Shustova, *Chemical Reviews*, 2020, **120**, 8790-8813.
79. Y. Liu, X. Guan and Q. Fang, *Aggregate*, 2021, **2**, e34.
80. J. Dong, P. Shen, S. Ying, Z.-J. Li, Y. D. Yuan, Y. Wang, X. Zheng, S. B. Peh, H. Yuan, G. Liu, Y. Cheng, Y. Pan, L. Shi, J. Zhang, D. Yuan, B. Liu, Z. Zhao, B. Z. Tang and D. Zhao, *Chemistry of Materials*, 2020, **32**, 6706-6720.
81. Y. Cui, B. Chen and G. Qian, in *Metal-Organic Frameworks for Photonics Applications*, eds. B. Chen and G. Qian, Springer Berlin Heidelberg, Berlin, Heidelberg, 2014, DOI: 10.1007/430_2013_133, pp. 27-88.
82. D. D. La, S. V. Bhosale, L. A. Jones and S. V. Bhosale, *ACS Applied Materials & Interfaces*, 2018, **10**, 12189-12216.
83. L. Yu, H. Wang, W. Liu, S. J. Teat and J. Li, *Crystal Growth & Design*, 2019, **19**, 6850-6854.
84. Q. Gong, Z. Hu, B. J. Deibert, T. J. Emge, S. J. Teat, D. Banerjee, B. Mussman, N. D. Rudd and J. Li, *Journal of the American Chemical Society*, 2014, **136**, 16724-16727.
85. W. P. Lustig, F. Wang, S. J. Teat, Z. Hu, Q. Gong and J. Li, *Inorganic Chemistry*, 2016, **55**, 7250-7256.
86. Z. Hu, W. P. Lustig, J. Zhang, C. Zheng, H. Wang, S. J. Teat, Q. Gong, N. D. Rudd, and J. Li, *Journal of the American Chemical Society*, 2015, **137**, 16209–16215
87. Z. Hu, G. Huang, W. P. Lustig, F. Wang, H. Wang, S. J. Teat, D. Banerjee, D. Zhang and J. Li, *Chemical Communications*, 2015, **51**, 3045-3048.
88. W. P. Lustig, S. J. Teat and J. Li, *Journal of Materials Chemistry C*, 2019, **7**, 14739-14744.
89. W. P. Lustig, Z. Shen, S. J. Teat, N. Javed, E. Velasco, D. M. O'Carroll and J.Li, *Chemical Science*, 2020, **11**, 1814-1824.
90. Z.-F. Wu, B. Tan, Z.-H. Fu, E. Velasco, X.-W. Liu, S. J. Teat, K. Zhu, K. Xing, X.-Y. Huang and J. Li, *Chemical Science*, 2022, **13**, 1375-1381.
91. F. Wang, Z. Zhou, W. Liu, L. Zhou, L. Chen and J. Li, *Dalton Transactions*, 2017, **46**, 956-961.
92. S.-S. Zhao, H. Zhang, L. Wang, L. Chen and Z. Xie, *Journal of Materials Chemistry C*, 2018, **6**, 11701-1706.
93. X. Hu, Z. Wang, B. Lin, C. Zhang, L. Cao, T. Wang, J. Zhang, C. Wang and W. Lin, *Chemistry – A European Journal*, 2017, **23**, 8390-8394.
94. H. Miyasaka, *Accounts of Chemical Research*, 2013, **46**, 248-257.
95. M. C. So, G. P. Wiederrecht, J. E. Mondloch, J. T. Hupp and O. K. Farha, *Chemical Communications*, 2015, **51**, 3501-3510.
96. M.-X. Yu, C.-P. Liu, Y.-F. Zhao, S.-C. Li, Y.-L. Yu, J.-Q. Lv, L. Chen, F.-L. Jiang and M.-C. Hong, *Angewandte Chemie International Edition*, 2022, **61**, e202201590.
97. M.-S. Wang, S.-P. Guo, Y. Li, L.-Z. Cai, J.-P. Zou, G. Xu, W.-W. Zhou, F.-K. Zheng and G.-C. Guo, *Journal of the American Chemical Society*, 2009, **131**, 13572-13573.
98. Y. Xu, L. Li, S. Zhang, S. Zhao and J. Luo, *Crystal Growth & Design*, 2016, **16**, 406-411.
99. C. Peng, Z. Zhuang, H. Yang, G. Zhang and H. Fei, *Chemical Science*, 2018, **9**, 1627-1633.
100. M. A. A. Al-Nubi, A. M. Hamisu, F. Y. Wardana, A. Ariffin, H. Jo, K. M. Ok and A. C. Wibowo, *Crystal Growth & Design*, 2019, **19**, 6274-6282.
101. X.-L. Lin, B. Chen, Y.-R. Huang, K.-Y. Song, P.-K. Zhou, L.-L. Zong, H.-H. Li, Z.-R. Chen and R. Jiang, *Inorganic Chemistry Frontiers*, 2020, **7**, 4477-4487.
102. C. Peng, X. Song, J. Yin, G. Zhang and H. Fei, *Angewandte Chemie*, 2019, **131**, 7900-7904.
103. J. He, M. Zeller, A. D. Hunter and Z. Xu, *Journal of the American Chemical Society*, 2012, **134**, 1553-1559.
104. M. Usman, S. Mendiratta, S. Batjargal, G. Haider, M. Hayashi, N. Rao Gade, J.-W. Chen, Y.-F. Chen and K.-L. Lu, *ACS Applied Materials & Interfaces*, 2015, **7**, 22767-22774.
105. O. Toma, M. Allain, F. Meinardi, A. Forni, C. Botta and N. Mercier, *Angewandte Chemie International Edition*, 2016, **55**, 7998-8002.
106. R. Li, S.-H. Wang, Z.-F. Liu, X.-X. Chen, Y. Xiao, F.-K. Zheng and G.-C. Guo, *Crystal Growth & Design*, 2016, **16**, 3969-3975.
107. É. Whelan, F. W. Steuber, T. Gunnlaugsson and W. Schmitt, *Coordination Chemistry Reviews*, 2021, **437**, 213757.
108. Y. Zhao and D. Li, *Journal of Materials Chemistry C*, 2020, **8**, 12739-12754.
109. C. Zhang, Z.-P. Yan, X.-Y. Dong, Z. Han, S. Li, T. Fu, Y.-Y. Zhu, Y.-X. Zheng, Y.-Y. Niu and S.-Q. Zang, *Advanced Materials*, 2020, **32**, 2002914.
110. H.-Q. Yin and X.-B. Yin, *Accounts of Chemical Research*, 2020, **53**, 485-495.
111. Y.-M. Wang, Z.-R. Yang, L. Xiao and X.-B. Yin, *Analytical Chemistry*, 2018, **90**, 5758-5763.
112. L. Qiu, C. Yu, X. Wang, Y. Xie, A. M. Kirillov, W. Huang, J. Li, P. Gao, T. Wu, X. Gu, Q. Nie and D. Wu, *Inorganic Chemistry*, 2019, **58**, 4524-4533.
113. Z. Sun, A. Khurshid, M. Sohail, W. Qiu, D. Cao and S.-J. Su, *Nanomaterials*, 2021, **11**, 2761.
114. U. Ryu, H. S. Lee, K. S. Park and K. M. Choi, *Polyhedron*, 2018, **154**, 275-294.
115. Z. Wang, C.-Y. Zhu, J.-T. Mo, P.-Y. Fu, Y.-W. Zhao, S.-Y. Yin, J.-J. Jiang, M. Pan and C.-Y. Su, *Angewandte Chemie International Edition*, 2019, **58**, 9752-9757.
116. M. Gutiérrez, Y. Zhang and J.-C. Tan, *Chemical Reviews*, 2022, **122**, 10438-10483.

117. Y. Cui, T. Song, J. Yu, Y. Yang, Z. Wang and G. Qian, *Advanced Functional Materials*, 2015, **25**, 4796-4802.
118. Z. Wang, Z. Wang, B. Lin, X. Hu, Y. Wei, C. Zhang, B. An, C. Wang and W. Lin, *ACS Applied Materials & Interfaces*, 2017, **9**, 35253-35259.
119. Y. Wen, T. Sheng, X. Zhu, C. Zhuo, S. Su, H. Li, S. Hu, Q.-L. Zhu and X. Wu, *Advanced Materials*, 2017, **29**, 1700778.
120. D. Samanta, P. Verma, S. Roy and T. K. Maji, *ACS Applied Materials & Interfaces*, 2018, **10**, 23140-23146.
121. X.-Y. Liu, K. Xing, Y. Li, C.-K. Tsung and J. Li, *Journal of the American Chemical Society*, 2019, **141**, 14807-14813.
122. X.-Y. Liu, Y. Li, C.-K. Tsung and J. Li, *Chemical Communications*, 2019, **55**, 10669-10672.
123. Y. Chen, B. Yu, Y. Cui, S. Xu and J. Gong, *Chemistry of Materials*, 2019, **31**, 1289-1295.
124. Y. Tang, W. Cao, L. Yao, Y. Cui, Y. Yu and G. Qian, *Journal of Materials Chemistry C*, 2020, **8**, 12308-12313.
125. A. Wang, Y.-L. Hou, F. Kang, F. Lyu, Y. Xiong, W.-C. Chen, C.-S. Lee, Z. Xu, A. L. Rogach, J. Lu and Y. Y. Li, *Journal of Materials Chemistry C*, 2019, **7**, 2207-2211.
126. Y. Lu, S. Wang, K. Yu, J. Yu, D. Zhao and C. Li, *Microporous and Mesoporous Materials*, 2021, **319**, 111062.
127. C.-Y. Sun, X.-L. Wang, X. Zhang, C. Qin, P. Li, Z.-M. Su, D.-X. Zhu, G.-G. Shan, K.-Z. Shao, H. Wu and J. Li, *Nature Communications*, 2013, **4**, 2717.
128. S.-R. Zhang, G.-J. Xu, W. Xie, Y.-H. Xu and Z.-M. Su, *Inorganic Chemistry Communications*, 2021, **123**, 108359.
129. W. Xie, J.-S. Qin, W.-W. He, K.-Z. Shao, Z.-M. Su, D.-Y. Du, S.-L. Li and Y.-Q. Lan, *Inorganic Chemistry Frontiers*, 2017, **4**, 547-552.
130. W. Xie, W.-W. He, D.-Y. Du, S.-L. Li, J.-S. Qin, Z.-M. Su, C.-Y. Sun and Y.-Q. Lan, *Chemical Communications*, 2016, **52**, 3288-3291.
131. X. Sun and Y. Lei, *TrAC Trends in Analytical Chemistry*, 2017, **89**, 163-180.
132. J. Liu, R. Li and B. Yang, *ACS Central Science*, 2020, **6**, 2179-2195.
133. A. Wang, Y.-L. Hou, F. Kang, F. Lyu, Y. Xiong, W.-C. Chen, C.-S. Lee, Z. Xu, A. L. Rogach, J. Lu and Y. Y. Li, *Journal of Materials Chemistry C*, 2019, **7**, 2207-2211.
134. Y. He, Y.-L. Hou, Y.-L. Wong, R. Xiao, M.-Q. Li, Z. Hao, J. Huang, L. Wang, M. Zeller, J. He and Z. Xu, *Journal of Materials Chemistry A*, 2018, **6**, 1648-1654.
135. W. Ying, Y. Mao, X. Wang, Y. Guo, H. He, Z. Ye, S.-T. Lee and X. Peng, *ChemSusChem*, 2017, **10**, 1346-1350.
136. S. Wu, D. Ren, K. Zhou, H.-L. Xia, X.-Y. Liu, X. Wang and J. Li, *Journal of the American Chemical Society*, 2021, **143**, 10547-10552.
137. D. Ren, H.-L. Xia, K. Zhou, S. Wu, X.-Y. Liu, X. Wang and J. Li, *Angewandte Chemie International Edition*, 2021, **60**, 25048-25054.
138. G. Han, S. Wu, K. Zhou, H.-L. Xia, X.-Y. Liu and J. Li, *Inorganic Chemistry*, 2022, **61**, 3363-3367.
139. W. J. Newsome, S. Ayad, J. Cordova, E. W. Reinheimer, A. D. Campiglia, J. K. Harper, K. Hanson and F. J. Uribe-Romo, *Journal of the American Chemical Society*, 2019, **141**, 11298-11303.
140. N.-C. Chiu, K. T. Smith and K. C. Stylianou, *Coordination Chemistry Reviews*, 2022, **459**, 214441.
141. A. K. Chaudhari and J. C. Tan, *Advanced Optical Materials*, 2020, **8**, 1901912.
142. M. Gutiérrez, C. Martín, M. Van der Auweraer, J. Hofkens and J. C. Tan, *Advanced Optical Materials*, 2020, **8**, 2000670.
143. T. Mondal, S. Mondal, S. Bose, D. Sengupta, U. K. Ghorai and S. K. Saha, *Journal of Materials Chemistry C*, 2018, **6**, 614-621.
144. Y. Fang, W. Liu, S. J. Teat, G. Dey, Z. Shen, L. An, D. Yu, L. Wang, D. M. O'Carroll and J. Li, *Advanced Functional Materials*, 2017, **27**, 1603444.